Great Lakes Microscopy Society Annual Meeting



Michigan Technological University, Houghton
October 9, 2026

Great Lakes Microscopy Society Annual Meeting, 9 October 2026

8:00 – 8:30 ***Registration & Check-in with Coffee/Light Refreshments***

8:30 - 8:40 ***Introductions & Meeting Program Overview*** (Dr. Ellen Keene, DuPont – GLMS Annual Meeting Program Chair)

8:40 - 8:50 ***Welcoming Remarks*** (Elizabeth Fraki, Director of Materials Characterization & Fabrication Facility, Michigan Technological University)

8:50-9:00 ***Opening Remarks*** (Andrew Barnard, Vice President for Research, Michigan Technological University)

Session 1, Biological Sciences: session chairs: Dr. Vickie Kimler, Oakland/Wayne State Universities (Retired) / Dr. Carol Heckman, Bowling Green State University

9:00 - 9:30 ***Invited Speaker*** Dr. Caryn Heldt (Michigan Technological University) – *The Study of Soft Biomaterials with AFM*

9:30 – 10:00 ***Invited Speaker*** Dr. Kevin Eliceiri (University of Wisconsin, Madison) - *Computational Imaging of the Tumor Microenvironment*

10:00 – 10:30 ***Invited Speaker*** Dr. Wei Zhang (University of Minnesota) - *Characterization of materials and biological samples by transmission electron microscopy*

10:30 – 10:45 ***Break***

10:45 –11:00 ***Student Platform*** Linqi Huang (University of Michigan), *Quantitative Imaging of Structure and Viability in Staphylococcus epidermidis-Infected Fibrin Clots Under Heated Perfusate*

11:00-11:15 ***Student Platform*** Oscar Moreno (University of Michigan), *Scanning Electron Microscopy Characterization of Surface Coverage and Thrombus Infiltration in Novel Coated ePTFE Vascular Grafts*

11:15-11:30 ***Student Platform*** Majid Rostami (Michigan Technological University), *Spatiotemporal Analysis of FAK Phosphorylation and Vinculin Dynamics Reveals Two Distinct Stiffness-Dependent Mechanotransduction Pathways in Cancer Cells*

11:30 – 12:30 ***Lunch Break & GLMS Society Business Meeting*** (Dr. Tao Ma, University of Michigan - GLMS President)

12:30 – 2:00 ***Poster Session & Vendor Showcase, Optional MCFF tours***

Session 2, Physical Sciences: session chair: Zehao Li, University of Michigan

2:00 – 2:30 ***Invited Speaker*** Dr. Sriram Vijayan (Michigan Technological University), *Unlocking the Mechanisms of Phase Transformations in Complex Metallic Alloys via In Situ TEM Heating – From Sample Preparation to Temperature Calibration and Data Interpretation*

2:30 – 3:00 ***Invited Speaker*** Dr. Xiaobing Hu (Northwestern), *Gas Cell TEM and Its Applications in Materials Science*

3:00 - 3:30 ***Invited Speaker*** Dr. Chia-Hao Lee (Cornell), *Advancing Electron Ptychography: From High-Performance Reconstruction to AI-Enhanced 3D Imaging*

3:30 – 3:45 ***Break***

3:45 – 4:00 ***Student Platform*** Jessica Ma (University of Michigan), *Graph Theoretical Relationships for Chiroptical Activity for Gold Nanorods with Complex Corrugated Geometry*

4:00 – 4:15 ***Student Platform*** Jason Manassa (University of Michigan), *Damage of Beam-Sensitive Organics from Room Temperature to Liquid Helium*

4:15 – 4:30 ***Student Platform*** Hailey McKenna (University of Michigan), *Tailoring the plasmonic properties of InGa alloy nanoparticle arrays*

4:30 – 4:45 ***Vendor Platform Presentation*** Dr. Anahita Pakzad (Gatan/Ametek), *Advances in Detector Technologies for Materials Science: From Low-Dose Imaging to 4D STEM*

4:45-5:00 ***Vendor Platform Presentation*** Dr. Austin Wade (Thermo Fisher Scientific), *Super-X G3: Higher Light-Element Sensitivity and Faster Compositional Mapping at Analytical Beam Currents*

5:00-5:15 ***Vendor Platform Presentation*** Dr. Eric Hintsala (Bruker), *Evaluating the Brittle-to-Ductile Transition of Silicon by in situ Nanomechanics*

5:15-5:30 ***Awards Presentation*** (Dr. Ellen Keene, DuPont – GLMS Annual Meeting Program Chair)

5:30 – 5:45 ***Closing Remarks and Group Photo*** (Dr. Tao Ma, University of Michigan – GLMS President)

Platform Presentations

Physicochemical Properties of Biomacromolecules Measured by Atomic Force Microscopy

Caryn L. Heldt

Health Research Institute and Department of Chemical Engineering, Michigan Technological University, Houghton MI USA

Large biomacromolecules, like viruses and extracellular vesicle, continue to be explored as therapeutic entities for hard to treat diseases, like cancer, COVID, and muscular dystrophies. We study the stiffness and surface chemistry of biomacromolecules using atomic force microscopy to improve manufacturing and delivery of these therapeutic entities.

We are extremely interested in the interaction of adeno-associated virus (AAV). AAV is a therapy for diseases that contain a single-gene deletion or mutation and offer the change for a cure to the disease, not just a continuous therapy. One major scale-up challenge is the removal of empty or non-gene of interest containing AAV capsids. To better understand the differences in the empty and full AAV capsids, we have developed a single particle atomic force microscopy (AFM) method to measure the differences in charge and hydrophobicity of AAV capsids using functionalized AFM tips [1]. The single particle measurements give us not only average information, but also information about the heterogeneity of the virus population.

We are also looking at the changes in stiffness and size for enveloped viruses and extracellular vesicles. Immobilization of entities to measure chemical changes on the surface is difficult for lipid bound particles. We determined a method to immobilize the particles [2], and now we have used this to determine how particles stiffness and size change with purification method.

Overall, we are using AFM to improve the delivery and manufacturing of biomacromolecules to reduce costs and improve access to these lifesaving treatments.

References:

1. Heldt, C.L., O. Areo, P.U. Joshi, X. Mi, Y. Ivanova, and A. Berrill, *Empty and Full AAV Capsid Charge and Hydrophobicity Differences Measured with Single-Particle AFM.* Langmuir, 2023. **39**(16): p. 5641–5648.

2. Mercado Velez, B., V. Sharma, S. Kriz, E.T.F. Freitas, P. Goetsch, and C.L. Heldt, *Physical Changes of Biomacromolecules upon Covalent Surface Immobilization.* Langmuir, 2026. **42**(11): p. 8018–8031.



Dr. Caryn L. Heldt is the Executive Director of the Health Research Institute, the James and Lorna Mack Chair in Continuous Processing, Director of the NIH T32 Program at MTU, and a Professor in the Department of Chemical Engineering at Michigan Technological University. She received her PhD from North Carolina State University, and her lab is focused on the purification, inactivation, and stability of viral vectors.

Computational Imaging of the Tumor Microenvironment

*Yuming Liu, Michael S. Nelson, Jenu V. Chacko, Kevin W. Eliceiri***

Center for Quantitative Cell Imaging, University of Wisconsin-Madison, Madison, WI, USA, 53706

Interactions between cancer cells and their surroundings dynamically remodel the tumor microenvironment (TME), driving cancer onset, invasion, metastasis, and therapeutic resistance. Quantifying these interactions requires sophisticated, automated imaging approaches. Here, we present key advances from our laboratory in developing integrated, "smart" computational microscopy platforms designed for robust TME quantification across cell models, animal models, and patient histological sections. Our approach seamlessly pairs intrinsic contrasts, like endogenous cellular fluorescence, with cutting-edge extrinsic fluorescent labels. This data-driven microscopy integrates two core components:

1. **Advanced Multimodal Imaging:** Provides comprehensive spatial profiling of cells and the extracellular matrix (ECM) by leveraging multiphoton, second harmonic generation (SHG), fluorescence lifetime imaging (FLIM), LC-PolScope, and polychromatic polarization microscopy (PPM).
2. **Utilizing Open-Source Software Ecosystems:** Combines imaging software (Micro-Manager, Pycro-Manager, OpenScan, PyImageJ, Fiji/ImageJ, CellProfiler, QuPath) with specialized analysis pipelines (TrackMate, CurveAlign, CT-FIRE, TMEQuant and deep learning models).

We highlight two recent smart microscope platforms that bridge automated hardware control with real-time computational analysis to reveal novel insights into TME structural dynamics:

- **QPSC-PPM (QuPath Scope Control of Polychromatic Polarization Microscopy):** This system aids in the detection of tumor-associated collagen signatures (TACS)—a reported indicator of patient survival—directly from standard H&E stained slides without requiring additional collagen specific staining. The platform bridges QuPath for whole-slide analysis and annotation-driven acquisition, MicroManager for hardware control, and Python-based TMEQuant libraries for automated TACS computation. This adaptable framework is extensible to other ECM imaging modalities such as SHG and LC-PolScope.
- **DREAMS-FLIM/HDIM (Data Reactive Acquisition and Microscope Steering for Fluorescence Lifetime and Hyperdimensional Imaging Microscopy):** DREAMS is

an LLM Agent-assisted adaptive microscopy framework that integrates microscope hardware control with real-time image analysis, enabling dynamic, data-driven acquisition on measurements of cell morphology, metabolism, and cell-cell interactions. Using Model Context Protocol (MCP) to securely interface microscope controls (MicroManager) with analysis tools for advanced techniques like FLIM, HDIM and 3D single cell-tracking, we enable real-time metabolic and dynamic interaction analysis between cancer, immune, and stromal cells to advance CAR T-cell immunotherapy research.

While developed for cancer research, these open-source workflows offer an extensible toolkit for any spatio-temporal study of complex tissue architectures. Ultimately, bridging smart hardware control with automated analysis accelerates both the discovery of novel clinical biomarkers and our fundamental understanding of cell-matrix dynamics.



Kevin Eliceiri, Ph.D., is the RRF Walter H. Helmerich Professor of Medical Physics and Biomedical Engineering at the University of Wisconsin at Madison. He is an investigator in the Morgridge Institute for Research and member of the UW Carbone Cancer Center. He is also associate director of the McPherson Eye Research Institute and director of the Center for Quantitative Cell Imaging. His laboratory (known as the Laboratory for Optical and Computational Instrumentation (LOCI)) is a biophotonics research group dedicated to the development and application of optical and computational technologies for cell studies. They are contributing lead developers to several open-source imaging software packages including FIJI, ImageJ2 and μManager. His open hardware instrumentation efforts involve novel forms of polarization, laser scanning and multiscale imaging. Eliceiri has authored more than 300 scientific papers on various aspects of optical imaging, image analysis, cancer and live cell imaging

Characterization of materials and biological samples by transmission electron microscopy

Guichuan Yu[1], William Arndt[2], Nathanial Talledge[2], Louis Mansky[2,3], and Wei Zhang[2,3,4]

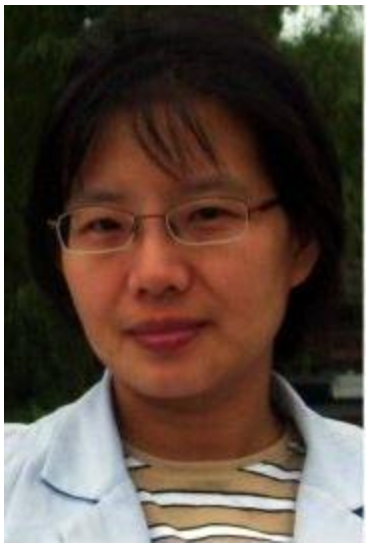
[1] Minnesota Supercomputing Institute, University of Minnesota, Minneapolis, MN. USA

[2] Institute for Molecular Virology, University of Minnesota, Minneapolis, MN. USA

[3] Department of Diagnostic and Biological Sciences, University of Minnesota, Minneapolis, MN.USA

[4] Characterization Facility, University of Minnesota, Minneapolis, MN. USA

Transmission electron microscopy (TEM) enables structural characterization of materials and biological specimens at nanometer to near-atomic resolution. Cryo-electron tomography (cryo-ET) and subtomogram averaging (StA) provide three-dimensional structural information regarding the pleomorphic nature of retrovirus Gag lattices. However, quantitative characterization of Gag lattice organization, including membrane coverage and curvature, requires accurate lattice coordinate identification and computational analyses beyond conventional StA workflows. We have developed a computational pipeline for the quantitative analysis of the retroviral Gag lattice structure by integrating coordinate refinement, particle quality assessment, and geometric analysis to generate reliable measurements of lattice organization. Following iterative subtomogram alignment, candidate Gag hexamer positions are evaluated using lattice surface continuity, local surface normal consistency, neighborhood consistency, and duplicate assignment criteria to remove false-positive and poorly aligned particles. High-confidence lattice coordinates are subsequently used to identify contiguous lattice regions underlying the viral membrane. Membrane coverage is quantified by calculating the area occupied by connected Gag lattice regions. The local lattice curvature is determined from spatial relationships among neighboring hexamers. The workflow was applied to analyzing immature human immunodeficiency virus type 2 (HIV-2) and human T-cell leukemia virus type 1 (HTLV-1) particles, revealing distinct Gag lattice architectures between these two human retroviruses. For HIV-2, the analysis enabled robust estimation of extensive Gag lattice coverage. For HTLV-1, curvature analysis revealed substantial local variability within individual particles, providing deeper insights into variable lattice morphology. This approach provides a general strategy for combining StA with spatial and geometric analyses to enable quantitative characterization of pleomorphic macromolecular assemblies.



Dr. Zhang obtained her PhD in the Structural Biology group at Purdue University and is currently an Associate Professor at the University of Minnesota. Her research focuses on the application of cryo-EM and cryo-ET methods to elucidate virus structures and the dynamic changes of viral proteins during infection. Her work centers on the mechanisms of enveloped virus assembly and membrane fusion, two critical stages of the viral life cycle.

Unlocking the Mechanisms of Phase Transformations in Complex Metallic Alloys via In Situ TEM Heating – From Sample Preparation to Temperature Calibration and Data Interpretation

Sriram Vijayan

Materials Science & Engineering, Michigan Technological University

In situ electron microscopy-based heating experiments are a well-established approach to observe thermally activated processes in metallic alloys used for structural applications [1-3]. Micro-electro-mechanical systems (MEMS)-based heating stages are the current 'state of the art' for in situ experiments in the transmission electron microscope (TEM) [4]. The principle of heat generation in these MEMS-based micro-heaters is Joule heating [2]. The small thermal mass of the micro-heater combined with the ability to heat and cool samples rapidly has enabled the ability to observe the various stages of a phase transformation at high spatial resolution compared to conventional furnace-based heating stages. However, the use of these MEMS-based micro heaters to obtain reliable and reproducible results are non-trivial [4-6].

In this talk, I will discuss the various limitations and challenges associated with the use of MEMS-based heating stages including TEM lamella preparation, temperature calibration of the micro heaters, specimen temperature measurement and data interpretation. Finally, in situ TEM observations of dynamic processes in a range of metallic alloy systems in the bulk and/or nanoparticulate form will be discussed.

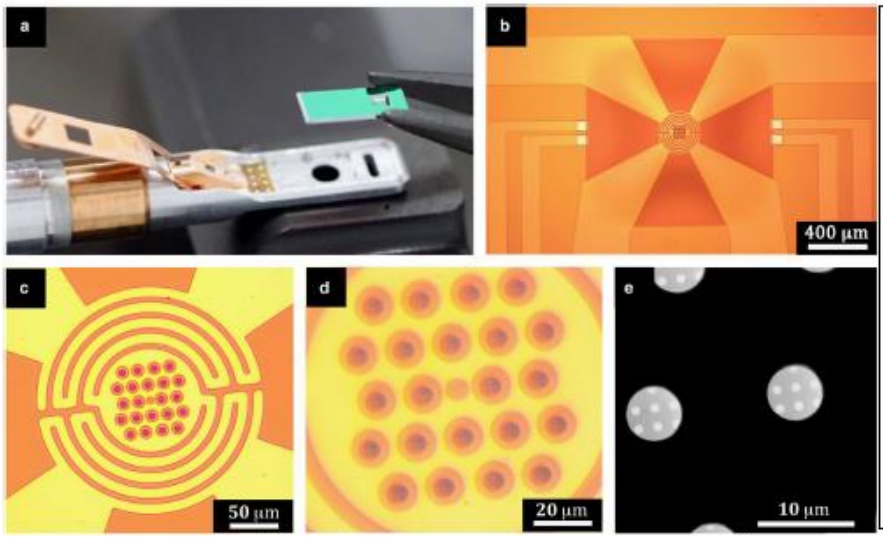


Figure 1. MEMs-based heating device for the FEI Nano-Ex/iV heating holder: (a) chip placement in the holder; (b–d) visible light microscopy images showing: (b) the electrical contacts, (c) the micro-heater plate, (d) the twenty-two 5 µm-diameter windows in the plate. e: Secondary electron image of the 15nm thick amorphous silicon nitride membrane across the windows. Figure reproduced from [5].

References

[1] S Vijayan, PhD Theses, 2018, University of Connecticut.

[2] S Vijayan et al., J. Mater. Sci. 54 (2019), p. 9921.

[3] H Leonard et al., Mater. Charact. 178 (2021), p. 111239.

[4] S Vijayan and M Aindow, Ultramicroscopy 196 (2019), p. 142.

[5] S Vijayan et al., Microsc. Res. Techn. (2021) p. 1.

[6] S Vijayan et al., Microsc. & Microanal., 23 (2017), p. 708.



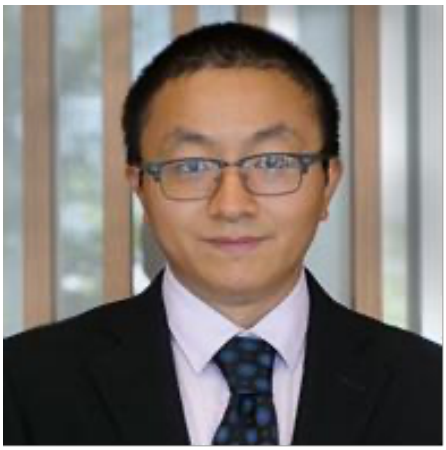
Sriram Vijayan is an Assistant Professor in the Department of Materials Science & Engineering at Michigan Technological University. Prior to joining Michigan Tech, Sriram worked a Research Associate in the Department of Materials Science & Engineering at The Ohio State University. He obtained his Ph.D. in Material Science and Engineering from the University of Connecticut (UConn). Sriram graduated with a Master's degree in Metallurgical & Materials Engineering from the Indian Institute of Technology-Madras, Chennai. His research group has three thrusts - understand thermally activated phenomena in structural materials utilizing microscopy-based tools, understanding process-structure property relationships in additively manufactured metallic components, and developing novel alloys for extreme environments. He is an active member of The Minerals, Metals and Materials Society (TMS) and Microscopy Society of America (MSA) and American Society for Testing and Materials (ASTM), American Society for Metals (ASM).

Gas Cell TEM and Its Applications in Materials Science

Xiaobing Hu

Northwestern University

Gas cell TEM enables real-time, atomic-scale observation of materials in reactive gas environments, offering direct insight into catalysis, nanoparticle evolution, and materials degradation. Its performance, however, is limited by electron scattering from conventional 50 nm SiNx windows. This talk presents the design and fabrication of sub-10 nm SiNx membranes that markedly improve imaging, spectroscopy, and diffraction in operando experiments. It then applies them to hydrogen dynamics in Pd nanocubes, Pd-catalyzed water formation, and MXene oxidation under O_2 and H_2O.



Dr. Xiaobing Hu holds the position of Research Associate Professor in the Materials Science and Engineering Department at Northwestern University, where he also serves as the TEM Facility Manager at the NUANCE Center. His research focuses on the advanced applications of various transmission electron microscopy (TEM) techniques across diverse scientific fields, including engineering alloys, energy materials, biominerals, and functional nanomaterials. Dr. Hu boasts a publication record of over 130 journal articles, with an H-index > 41.

Advancing Electron Ptychography: From High-Performance Reconstruction to AI-Enhanced 3D Imaging

Chia-Hao Lee

Cornell University

Electron ptychography has emerged as a powerful technique for atomic-resolution imaging, but its widespread adoption has been limited by computational barriers and fundamental depth resolution challenges. We address these limitations through two complementary advances. First, to overcome computational bottlenecks, we developed a suite of high-performance reconstruction tools. This includes PtyRAD, an open-source iterative framework leveraging automatic differentiation and GPU acceleration that achieves a 24× speedup over existing tools, democratizing access with over 13,000 downloads and adoption by major semiconductor manufacturers. Complementing this, we introduce fast-acbf, a GPU-accelerated direct solver enabling near real-time ptychography optimized for low-dose and biological samples. Second, we developed MEP-Diffusion, integrating generative diffusion models with multislice electron ptychography to overcome fundamental depth resolution limits. By learning structural priors from large crystal structure databases, this approach enables 3D atomic structure determination from single-tilt acquisitions, transforming ptychography from a primarily 2D technique into a high-throughput 3D characterization tool. Together, these advances establish a complete pipeline from real-time feedback and efficient reconstruction to enhanced depth sensitivity, positioning electron ptychography as a versatile tool for quantitative 3D characterization, spanning from high-resolution biological imaging to atomic-scale materials analysis.



Dr. Chia-Hao Lee is a 2023–2026 Eric and Wendy Schmidt AI for Science Postdoctoral Fellow. Working with Prof. David Muller at Cornell University, his primary research interests center on advanced computational electron microscopy, specifically focusing on ptychography and 4D-STEM. He received his PhD from the University of Illinois Urbana-Champaign under Prof. Pinshane Huang. By incorporating machine learning techniques into microscopy workflows, his research aims to enable high-resolution, high-throughput, and reliable characterization of materials at the atomic scale.

Quantitative Imaging of Structure and Viability in *Staphylococcus epidermidis*-Infected Fibrin Clots Under Heated Perfusate

Linqi Huang[1,3], Michael J. Solomon[1,3,] and J. Scott VanEpps[2,3,4,*]*

[1] Department of Chemical Engineering, University of Michigan, Ann Arbor, Michigan, USA
[2] Department of Emergency Medicine, University of Michigan, Ann Arbor, Michigan, USA
[3] Biointerfaces Institute, University of Michigan, Ann Arbor, Michigan, USA
[4] Department of Molecular, Cellular, and Developmental Biology, University of Michigan, Ann Arbor, Michigan, USA

Central line-associated bloodstream infections (CLABSI) are a major cause of illness and rising healthcare costs in hospitalized patients. These infections often begin when bacteria, commonly *Staphylococcus epidermidis*, colonize a blood clot that forms around a catheter, creating an infected clot known as septic thrombus.[1] Bacteria embedded within this thrombus are shield by both the extracellular polymeric substance they secrete and the surrounding fibrin network, protecting them from antibiotics and the host immune response. The current standard of care for an infected catheter is often catheter removal, which is invasive, costly and not always feasible in critically ill patients. As a less invasive, catheter-salvage alternative, we are investigating heated perfusate, delivered directly through the catheter, as a means of killing bacteria embedded within the fibrin clot in situ. However, it remains unclear how heat and shear stress affect the physical structure and bacterial viability of the infected clot. This information is important for predicting treatment efficacy and the risk of clot fragmentation.

To investigate this question, we developed an in vitro model of a septic thrombus by forming thrombin-initiated fibrin clots seeded with *Staphylococcus epidermidis*, then delivering heated perfusate across a physiologically relevant temperature range (37, 45, 50 and 60°C) using a fluidic device.[2, 3] Three-channel confocal fluorescence microscopy was used to capture live cells, dead cells and fibrin network separately, and image analysis quantified overall bacterial viability within the clot, fibrin mesh size and the spatial progression of viability loss with increasing perfusate temperature. To resolve where within a biofilm colony bacterial cell death occurred, we further classified each colony's interior and peripheral regions (defined geometrically relative to a fitted colony radius) as live, dead, or cell-free based on local live/dead cell fractions.

Overall bacterial viability declined steadily with temperature, from 72% live at 37°C to 6% live at 60°C, while fibrin mesh size shrank from approximately 5 μm to 3 μm over the same range, indicating progressive densification of the clot structure. The spatial viability analysis showed that this loss of viability was not uniform within the colony. Bacterial death consistently initiated in the colony interior before spreading to the periphery, and at the highest temperatures dead material was progressively cleared from the colony core, leaving mostly cell-free interiors surrounded by a shell of dead cells.

These results demonstrate that heated perfusate progressively kills bacteria and compacts the fibrin network, and that bacterial death follows a distinct spatial trajectory, initiating in the colony interior and later clearing from the core, rather than occurring uniformly. These findings provide new mechanistic insight relevant to the design of catheter-salvage thermal treatment strategies for CLABSI.

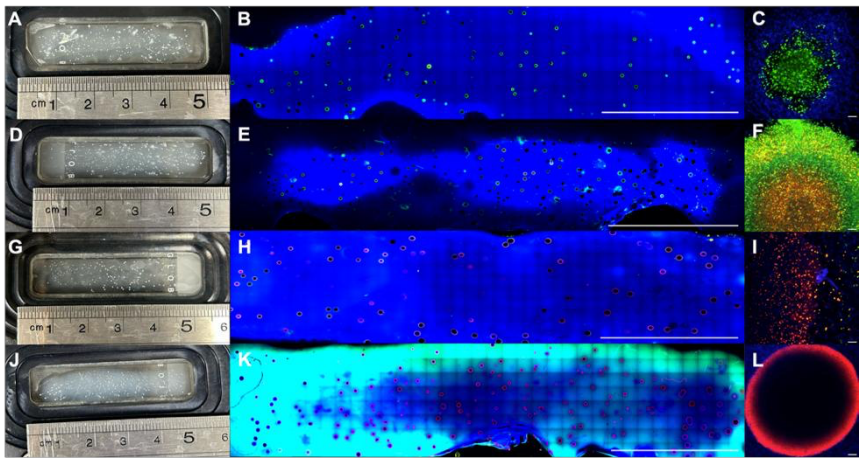


Fig. 1. Macroscopic images of infected fibrin clots (A, D, G, J), whole-clot fluorescence scans (B, E, H, K), and zoomed confocal images of representative bacterial colonies (C, F, I, L) after treatment with heated perfusate at 37, 45, 50, and 60°C. Green: live cells; red: dead cells; blue: fibrin. Scale bars: ruler markings in cm (A, D, G, J); 10,000 µm for panels B, E, H, K; 10 µm for panels C, F, I, L.

References:

1. Raad II, Luna M, Khalil SA, Costerton JW, Lam C and Bodey GP. *JAMA* (1994) 271 1014-1016.

https://doi.org/10.1001/jama.1994.03510370066034

2. Ma TM, VanEpps JS and Solomon MJ. *Biophysical Journal* (2017) 113 2100-2109.

https://doi.org/10.1016/j.bpj.2017.09.001

3. Beckwith JK, VanEpps JS and Solomon MJ. *Appl Environ Microbiol* (2020) 86 e01193-20.

https://doi.org/10.1128/AEM.01193-20

Scanning Electron Microscopy Characterization of Surface Coverage and Thrombus Infiltration in Novel Coated ePTFE Vascular Grafts

Oscar Moreno[1], Yanqing Zhao[1], Trevin Eggleston[1], Zachary Platte[1], Catherine Luke[1], Amber Clay[1], Daniel D. Myers[1, 2], Thomas Wakefield[1], Peter Henke[1], Andrea Obi[1].*

[1]Section of Vascular Surgery, Department of Surgery, University of Michigan. Ann Arbor, MI.

[2]Unit for Laboratory Animal Medicine, University of Michigan, Ann Arbor, MI.

Introduction: Peripheral artery disease affects approximately 8.5 million adults in the United States, and although open bypass remains an important revascularization strategy, prosthetic ePTFE grafts demonstrate limited long-term durability, with reported 5-year primary patency of approximately 52% for above-knee femoropopliteal bypass. (1–3) Functionalizing ePTFE vascular grafts improves hemocompatibility and long-term patency. Incomplete coverage exposes the thrombogenic fibrillar substrate, encouraging protein adsorption, platelet adhesion, thrombus formation, and graft failure. Effective modification needs a uniform, conformal coating that covers and penetrates the graft microarchitecture while preserving function.

Methods: We used scanning electron microscopy (SEM) to characterize the surface morphology of an experimental perfluorocarbon (PFC) coating on ePTFE vascular grafts and to examine structural features associated with graft thrombosis after implantation. Native commercial heparin-coated ePTFE grafts and grafts exposed to the PFC coating for 30 minutes or 24 hours, and explanted graft specimens, were examined by SEM at magnifications ranging from 50× to approximately 2,940×.

Results: In Native ePTFE grafts, SEM showed a highly porous structure. After 30 minutes of coating, irregular, smooth areas appeared, leaving much of the fibrillar ePTFE exposed. Extending to 24 hours produced larger, film-like regions that bridged gaps and covered pores, but the coating was uneven with exposed ePTFE. (**Fig.1A-C)**. No delamination, cracking, or bubbles were detected. SEM showed dense, irregular surface deposits on the implanted grafts, with an aggregated structure typical of thrombotic material. **(Fig.1D)** Cross-sectional examination also showed material extending into the internodal spaces within the porous graft wall, consistent with intramural thrombus infiltration. **(Fig.1E)** The underlying node-fibril architecture remained identifiable beneath portions of the surface deposits.

Conclusions: SEM effectively linked microscale coating heterogeneity with post-implantation graft thrombosis. Improved surface wetting, coating uniformity, and/or substrate modification may therefore be required to achieve more complete coverage and improve the hemocompatibility of porous ePTFE vascular grafts. Initial PFC coating prototyping failed to form a continuous, conformal layer over porous ePTFE, exposing fibrillar areas to blood and leading to thrombus formation and graft infiltration.

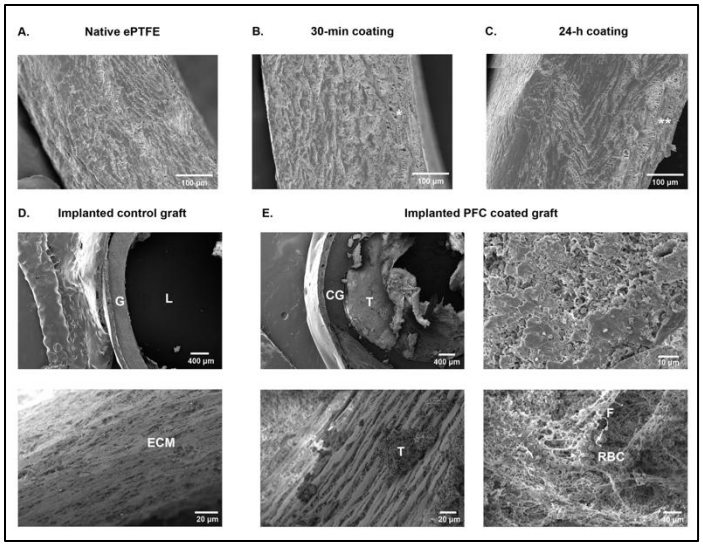


Fig. 1. SEM images show how coating duration affects ePTFE surface and grafts. **A.** Native ePTFE has a porous fibrillar structure. **B.** After 30 min, localized coating domains (*) with exposed fibrils. **C.** After 24 hours, broader film-like areas (**) partially cover the surface, but coating is uneven. **D.** Control graft shows preserved wall (G) and lumen (L), with ECM deposition. **E.** PFC-coated graft shows thrombotic material (T), with dense RBC and fibrin aggregates indicating surface thrombosis and infiltration. (CG), coated graft.

REFERENCES

1. Criqui MH, Matsushita K, Aboyans V, Hess CN, Hicks CW, Kwan TW, et al. Lower Extremity Peripheral Artery Disease: Contemporary Epidemiology, Management Gaps, and Future Directions: A Scientific Statement From the American Heart Association. Circulation. 2021 Aug 31;144(9):e171–91. doi:10.1161/CIR.0000000000001005 PubMed PMID: 34315230; PubMed Central PMCID: PMC9847212.

2. Vartanian SM, Conte MS. Surgical intervention for peripheral arterial disease. Circ Res. 2015 Apr 24;116(9):1614–28. doi:10.1161/CIRCRESAHA.116.303504 PubMed PMID: 25908732.

3. Klinkert P, Schepers A, Burger DHC, van Bockel JH, Breslau PJ. Vein versus polytetrafluoroethylene in above-knee femoropopliteal bypass grafting: five-year results of a randomized controlled trial. J Vasc Surg. 2003 Jan;37(1):149–55. doi:10.1067/mva.2002.86 PubMed PMID: 12514593.

Spatiotemporal Analysis of FAK Phosphorylation and Vinculin Dynamics Reveals Two Distinct Stiffness-Dependent Mechanotransduction Pathways in Cancer Cells

Majid Rostami[1] and Sangyoon J. Han[1,]*
[1]Department of Biomedical Engineering, Michigan Technological University, Houghton, MI, USA

Focal adhesion kinase (FAK) is a central signaling molecule at integrin-based adhesion complexes, yet a critical contradiction persists: while both FAK and RhoA activity increase with extracellular matrix (ECM) stiffness, FAK activation should suppress RhoA, the opposite of what occurs on stiff substrates. Structural studies suggest FAK may exist in two conformational states, a compact, chemically activated state that suppresses RhoA, and a force-extended state that activates it, but direct live-cell evidence has been lacking. We performed live-cell confocal imaging of cancer cells co-expressing a FRET-based pFAK biosensor (Y397 phosphorylation) and fluorescent vinculin (talin mechanosensitivity indicator) on soft (0.6 kPa) and stiff (6 kPa) substrates. Individual focal adhesions were detected using our training-free FADE algorithm, tracked from birth through turnover, and analyzed using Convergent Cross Mapping (CCM) to establish directional causal coupling between signals.

Analysis revealed striking heterogeneity: only 9% of adhesions showed coordinated vinculin-pFAK increases, while 20% showed vinculin decreasing as pFAK increased, demonstrating FAK activation independent of talin mechanosensing. CCM analysis showed that approximately 75% of causal vinculin-pFAK coupling concentrated at protruding cell edges on stiff substrates, with substantially weaker coupling on soft substrates. Most strikingly, pFAK assembly and disassembly rates were both significantly faster on soft substrates ($p < 0.001$), indicating rapid chemical turnover, while stiff substrates produced slower, sustained phosphorylation. Yet despite dramatically lower vinculin levels on soft substrates, pFAK reached comparable intensity levels across conditions. These results support a two-state model: on soft ECM, FAK undergoes rapid chemical activation with weak talin coupling (State 1), while on stiff ECM, mechanical forces produce sustained activation with strong causal coupling at protruding edges (State 2). This qualitative mechanistic switching may underlie the mechanical adaptability required for cancer metastasis and inform context-specific therapeutic strategies. [1]

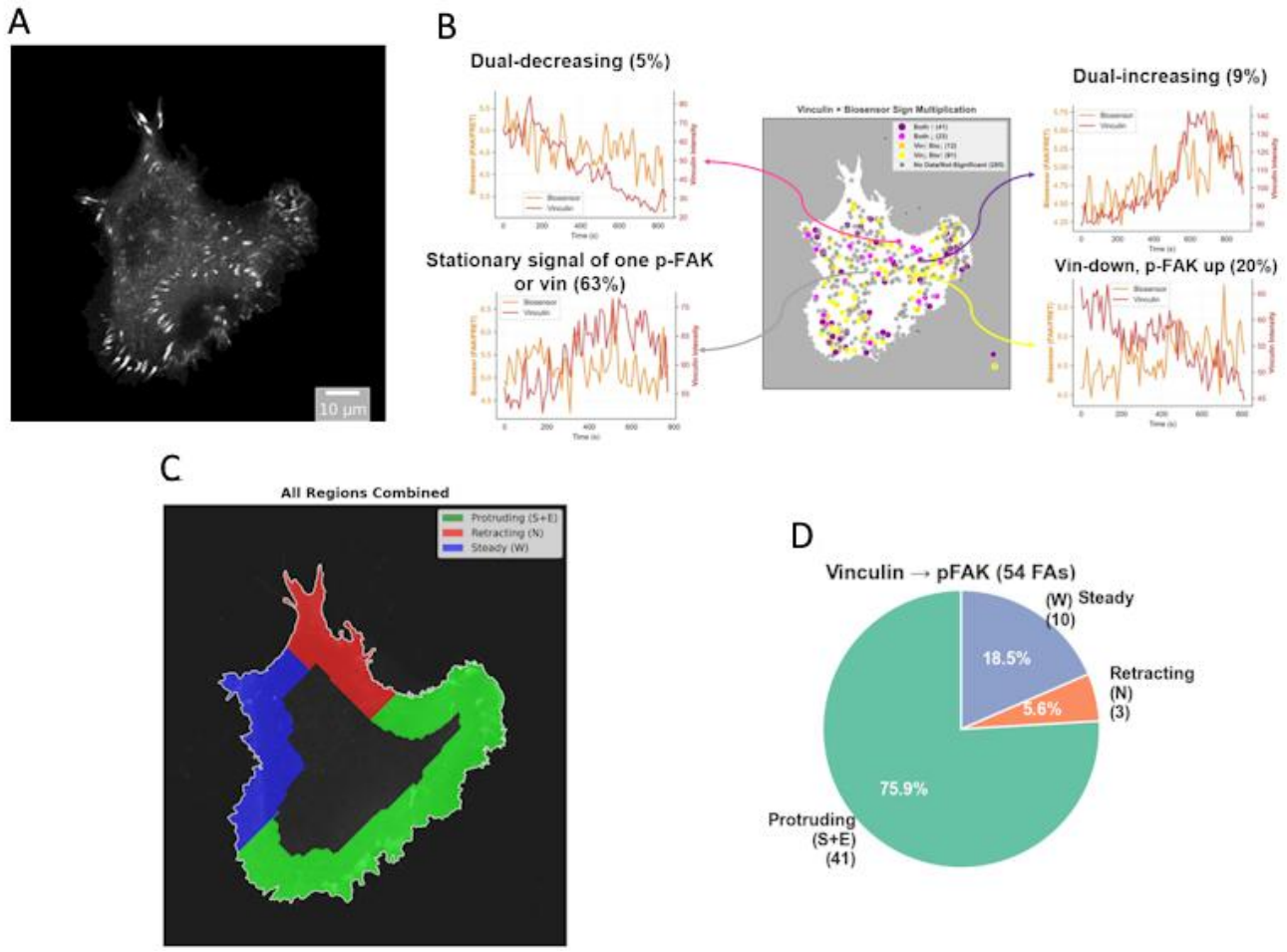


Fig. 1. Spatiotemporal analysis of FAK-vinculin signaling dynamics on soft (0.6 kPa) and stiff (6 kPa) substrates. (A) Raw pFAK biosensor image showing focal adhesion distribution. (B) Multi-channel signal extraction classifying individual adhesion signaling patterns: dual-increasing (9%), vinculin-down/pFAK-up (20%), dual-decreasing (5%), and stationary (63%). (C) CCM directional coupling distribution showing ~75% of causal coupling at protruding edges on stiff substrates.

References:

1. Bauer MS et al. *PNAS* (2019) **116** 6766-6774. https://doi.org/10.1073/pnas.1820567116

Graph Theoretical Relationships for Chiroptical Activity for Gold Nanorods with Complex Corrugated Geometry

Jessica Ma[1, 2, 3], Anjana Kannan[4], Yingying Cai[1, 2, 3], Andrés Serrano Freijeiro[5], Robin Girod[4], Valerio La Gambina[5], Luis M. Liz-Marzán[5,], Sara Bals[4,*], Nicholas A Kotov[1, 2, 3,*]*

[1]*Department of Chemical Engineering, University of Michigan; Ann Arbor, 48105, USA.*

[2]*Center of Complex Particle Systems (COMPASS), University of Michigan; Ann Arbor, 48105, USA*

[3]*Biointerfaces Institute, University of Michigan; Ann Arbor, 48105, USA*

[4]*EMAT and NANOlab Center of Excellence, University of Antwerp; Antwerp, 2020, Belgium*

[5]*CINBIO and Departamento de Química Física, Universidade de Vigo, Vigo 36310, Spain*

Chiral gold nanoparticles with wrinkled geometries can display high optical activity, comparable to or exceeding that of nearly perfectly shaped helicoids.[1] However, their partially stochastic structural patterns are difficult to quantify using standard order parameters; the relationship between the particles' complex shapes and their chiroptical characteristics are mathematically opaque.[2] Electron tomography reconstructions are converted into graphs embedded in Cartesian space in which edges represent the wrinkles, while nodes denote their junctions. This graph-theoretical framework can connect the intricate organization of wrinkled gold nanorods to their optical activity, while retaining the nanorods' local and global chirality and enabling the application of structural descriptors combining both topological and geometric characteristics. The size-adjusted edge-angle (SEA), a graph-based descriptor integrating topological and geometric parameters, reveals a near-perfect (R2 = 0.97) correlation with the maximum optical g-factor across multiple particle families, including chiral and achiral examples. The strong model fit between SEA and g-factor, retained for single-crystalline, pentatwinned and dumbbell-shaped gold nanorods, indicates that three-dimensional graphs capture the essential structural patterns which determine chiroptical function in plasmonic matter, which emerges from the combined effects of chiral wrinkle orientation, the density of surface features, and the variable orientations of the wrinkles.

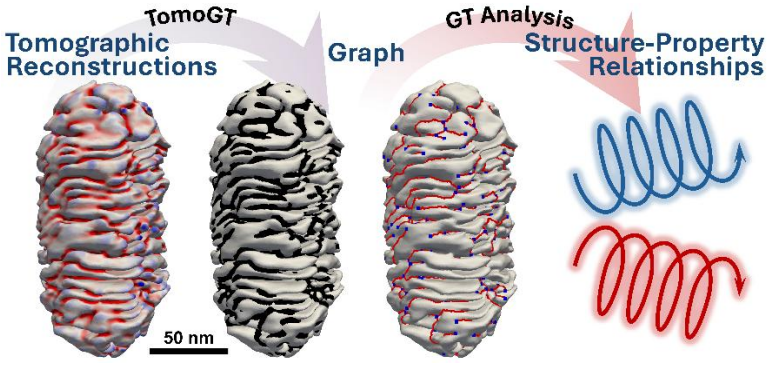


Fig. 1. Our TomoGT software allows us to extract graphs from tomographic reconstructions of complex gold nanorods, which in turn enables us to establish relationships between their wrinkle geometry and optical g-factor.

References:
1. G. González-Rubio et al. *Science* (2020) **368** 1472-1477.
https://doi.org/10.1126/science.aba0980
2. K. Van Gordon, R. Girod et al. *Nano Lett* (2025) **25 (7)** 2887–2893.
https://doi.org/10.1021/acs.nanolett.4c06145

Damage of Beam-Sensitive Organics from Room Temperature to Liquid Helium

Jason Manassa[1], Eric M. Orson[2], Nishkarsh Agarwal[1,3], Kaia Thompson[1], Alex Stangel[1], Ambarneil Saha[3], Peter Ercius[3], Maya Gates[4], Ismail El-Baggari[4], and Robert Hovden[1,2,4]
[1] University of Michigan, Material Science and Engineering, Ann Arbor, Michigan, USA
[2] University of Michigan, Applied Physics, Ann Arbor, Michigan, USA
[3] National Center for Electron Microscopy, Molecular Foundry, Lawrence Berkeley National Laboratory, Berkeley, California USA
[4] h-Bar Instruments, Ann Arbor, Michigan, USA

Electron beam damage continues to be a fundamental limitation in microscopy of beam-sensitive materials such as organics, MOFs, and batteries [1,2]. Since the earliest electron diffraction studies of organic crystals in the 1930s, paraffin wax has emerged as the canonical model for quantifying radiation damage due to its basic chain chemistry, well understood crystal structure, and rapid breakdown from electron beam exposure [3]. However, despite almost a century of investigation, the reported electron fluence limits for paraffin vary by over an order of magnitude, and its damage mechanisms remain elusive, raising unresolved questions regarding reproducibility and trustworthiness of "known" cryoprotection factors.

In this work, we begin by tracing the historical evolution of paraffin analysis in the electron microscope from its initial use in X-ray crystallography on the suggestion of Sir William Bragg in 1928, to its first use with electrons in 1936 through its contemporary use in liquid helium and ultrafast pulsed TEM [4,5]. A holistic review of the dozens of prior measurements highlights the substantial scatter in reported fluence limits across temperatures and operating voltages. As showcased in Figure 1, not only do the paraffin forms vary widely, but multiple independent studies using the same material, at the same temperature, under the same voltage, report fluence limits that differ by factors of 10 or higher, underscoring the lack of a systematic and standardized experimental framework.

To address this discrepancy, we leverage a high-stability side entry liquid-helium specimen holder [6] and the single electron event sensitive EMPAD detector. This methodology enables direct measurement of the total electron fluence per unit area while simultaneously tracking Bragg peak fading with both spatial and temporal precision. As shown in Figure 2, this approach allows us, at liquid helium temperatures, to resolve local Bragg peak fading associated with variations in internal structure and beam resilience. Resolving these local phenomena provides a new mechanistic basis for why prior measurements over the past century differ significantly, even when accounting for sample preparation [7].

Paraffin samples prepared using a consistent and transparent standard operating procedure are examined across multiple temperature regimes: room temperature, liquid nitrogen, and liquid helium. Our findings demonstrate a monotonic increase in the critical electron fluence as temperature decreases, with a large enhancement from cooling to liquid nitrogen and liquid helium. The exact multiplier of the cryoprotection factor is shown to depend on specimen thickness and beam conditions. These findings aim to reconcile

the seemingly sporadic findings of prior work.

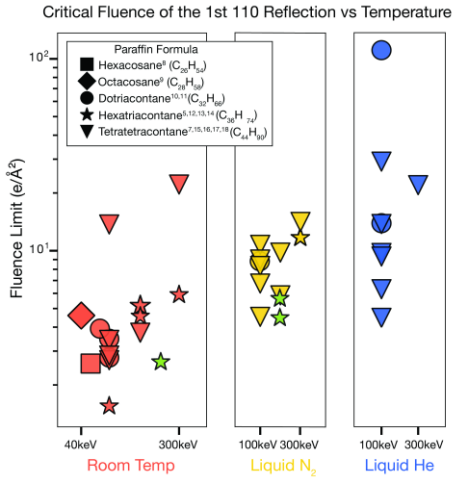


Fig. 1. Overview of prior paraffin electron fluence limit studies at various temperatures and voltages. Results vary widely, with some room temperature limits outperforming liquid helium, highlighting unreliability in data collection and/or sample preparation. Data from this work is highlighted in green.

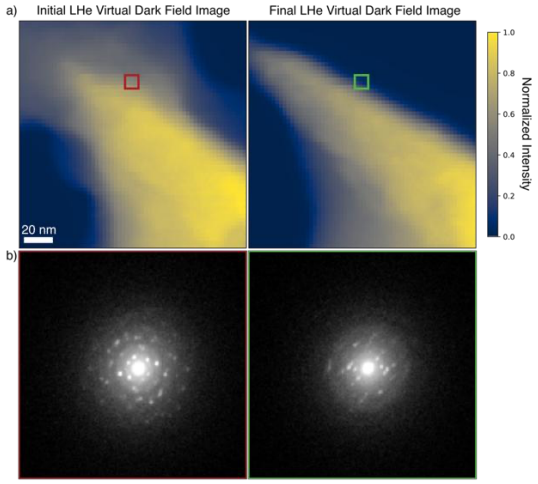


Fig. 2. Local variation in Bragg peak fading probed via 4D-STEM at liquid helium temperatures. a) 60x60 region of a 512x512 4D STEM virtual dark field image of paraffin (C_{36}) before (left) and after (right) damage due to electron beam exposure. b) Corresponding averaged diffraction patterns of 3x3 subregion shown in red and green bounding box respectively.

References:

1. Glaeser RM. *Ultramicroscopy* (**2025**) **271** 114118. https://doi.org/10.1016/j.ultramic.2025.114118
2. Egerton RF. *Micron* (**2019**) **119** 72–87. https://doi.org/10.1016/j.micron.2019.02.003
3. Rigamonti R. *Gazzetta Chimica Italia* (**1936**) **66** 174–176.
4. Muller A. *Proc. R. Soc. A* (**1928**) **120** 437–444. https://doi.org/10.1098/rspa.1928.0158
5. VandenBussche EJ and Flannigan DJ. *Nano Letters* (**2019**) **19** 6687–6694. https://doi.org/10.1021/acs.nanolett.9b03074
6. Gates M et al. *Microscopy and Microanalysis* (**2025**) **31** (Suppl. 1). https://doi.org/10.1093/mam/ozaf048.340
7. International Experimental Study Group (IESG). *J. Microscopy* (**1986**) **141** 385.

Tailoring the plasmonic properties of InGa alloy nanoparticle arrays

*Hailey McKenna[1], Catherine Huang[1], Tao Ma[2], and Rachel S. Goldman[1]**
[1]Department of Materials Science and Engineering, University of Michigan, Ann Arbor, MI, USA
[2]Michigan Center for Materials Characterization (MC)[2], University of Michigan, Ann Arbor, MI, USA

It has been shown that individual gallium and indium nanoparticles (NPs) generate localized surface plasmon resonances (LSPR) at energies of ~4 [1] and ~8 eV,[2] respectively. For pure indium NPs, air exposure induces the formation of a crystalline In_2O_3 shell that quenches the short-wavelength LSPR.[2] On the other hand, air-exposed gallium NPs develop a Ga_xO_y shell and still exhibit LSPR.[1] Therefore, to extend LSPRs to shorter wavelengths without quenching the DUV component, we consider arrays of bimetallic InGa NPs. A gallium-rich native oxide shell is observed on InGa NPs using scanning TEM (STEM) with x-ray dispersive spectroscopy (EDS). As indium composition (x_{In}) increases, so does shell thickness. We used monochromated electron energy loss spectroscopy (EELS) to investigate the LSPR of individual indium, gallium, and InGa NPs. EEL spectra collected from individual indium NPs following the removal of the oxide shell reveal LSPR energies between 5.3 and 8.0 eV depending on NP shape, size, and clustering. However, no LSPR is observed for indium NPs with an In_2O_3 shell. Interestingly, individual In-Ga and gallium NPs both exhibit LSPR between 5.6 and 6.2 eV. Therefore, the formation of a gallium-rich shell on InGa NPs can protect short-wavelength LSPR, supporting the promise of In-Ga NP arrays for deep-UV plasmonics.

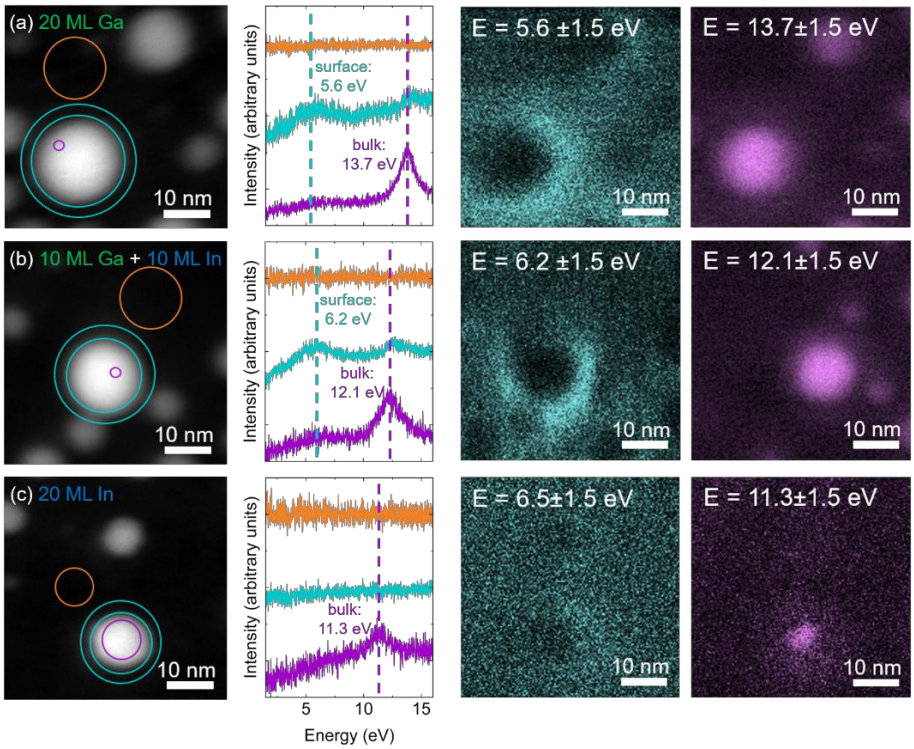


Fig. 1. ***By column:*** (left) STEM with (mid-left) corresponding EELS spectra and 2D energy maps of the (mid-right) LSP and (right) bulk plasmon. ***By row:*** For oxidized (a) gallium and (b) InGa NPs, LSPR peaks are observed at 5.6 and 6.2 eV, respectively. (c) For an oxidized indium NP, no LSPR is observed.

References:

1. de la Mata, M., Catalán-Gómez, S., Nucciarelli, F., Pau, J. L., and Molina, S. I. *Small* (2019) **15** 1902920. https://doi.org/10.1002/smll.201902920
2. McKenna, H. D. L., Shrestha, B., Lu, E., Lott, H., Subedi, I., Chen, X., Hwang, S., Zakharov, D., Podraza, N. J., Yang, J. C., and Goldman, R. S. *Appl. Phys. Lett.* (2025) **127** 031701. https://doi.org/10.1063/5.0271244

Advances in Detector Technologies for Materials Science: From Low-Dose Imaging to 4D STEM

Anahita Pakzad[1]
[1]*Gatan Inc., Pleasanton, CA, USA*
** Corresponding author: ana.pakzad@ametek.com*

Recent advances in electron detector technology are transforming transmission electron microscopy (TEM) from a primarily image-recording tool into a dose-efficient, high-throughput, and information-rich platform for materials science. This presentation reviews how improvements in sensor architecture, direct electron detection, electron counting, high-speed readout, and integrated acquisition software enable researchers to see weak signals, follow dynamic processes, and extract crystallographic, chemical, and spatially resolved information from beam-sensitive or rapidly evolving specimens.

The discussion begins with the evolution from film, CCD, and scintillator-coupled CMOS cameras to modern direct detection and hybrid-pixel detectors. Direct detection improves signal transfer by eliminating intermediate scintillator conversion, while electron counting further enhances image quality by suppressing read noise and reducing variability in electron energy deposition. These capabilities improve detective quantum efficiency and allow high-quality imaging and diffraction at substantially lower electron doses, which is critical for soft matter, beam-sensitive materials, low-dose structural studies, and long-duration experiments such as tomography and *in situ* microscopy.

Several application examples illustrate how detector performance directly affects scientific outcomes. High sensitivity and low background noise improve detection of weak diffraction spots, while high frame rates enable continuous acquisition for dynamic processes and reduce the impact of drift and beam damage. In 4D STEM, fast pixelated detectors shorten dwell times, expand accessible scan areas, and provide diffraction patterns with sufficient signal-to-noise for orientation mapping, strain mapping, differential phase contrast, virtual aperture imaging, and ptychographic reconstruction. Integrated hardware and software synchronization further enables multimodal workflows in which imaging, 4D STEM, EELS, energy-filtered diffraction, custom scan strategies, and scripting-based automation are linked within a common experimental environment.
Together, these developments demonstrate that modern TEM performance is increasingly defined not only by microscope optics, but also by detector sensitivity, speed, dynamic range, and software-enabled experiment design. By combining direct detection, electron counting, high-speed 4D STEM acquisition, dose awareness, and automated multimodal workflows, detector systems allow researchers to obtain more quantitative information from fewer electrons and to connect structure, chemistry, dynamics, and function with higher confidence.

Super-X G3: Higher Light-Element Sensitivity and Faster Compositional Mapping at Analytical Beam Currents

Austin Wade[1]
[1]*Thermo Fisher Scientific, Hillsboro, OR, 97124, USA*

Energy-dispersive X-ray spectroscopy (EDS) in the transmission electron microscope is essential for nanoscale compositional analysis, but detector electronics can impose a trade-off between spectral resolution and throughput. At the high X-ray count rates used for fast, large-area mapping and compositional tomography, detector dead time limits usable signal, while faster processing settings can degrade energy resolution.

This presentation introduces the Super-X G3 EDS system and demonstrates how its redesigned pulse-processing electronics eliminates the need for compromise when performing analytical experiments. Performance is compared directly with the established Super-X G2 detector using count-rate measurements, equal-current spectra from LaB_6, and spectrum imaging of an Al-Cu-Li alloy. Across a broad count-rate range, optimized G3 processing substantially reduces dead time while maintaining stable or improved energy resolution. Light element sensitivity is greatly improved with G3 producing approximately six times greater B Kα peak intensity than G2 while reducing the B-peak full width at half maximum, demonstrating improved signal with higher energy resolution. In a high probe current analytical EDS mapping comparison, G3 operated at 15% dead time compared with 55% for G2 and delivered more than twice the signal across small Mn-rich precipitates.

These gains translate into stronger light-element sensitivity, more efficient use of high beam currents, and faster acquisition of high-quality elemental maps. The presentation will show how Super-X G3 can expand the practical application space for demanding 2D, 3D, and multimodal workflows, helping laboratories collect better compositional data in less time without sacrificing spectral performance.

Evaluating the Brittle-to-Ductile Transition of Silicon by *in situ* Nanomechanics

Eric D. Hintsala[1], Kevin M. Schmalbach[1] and Sanjit Bhowmick[1]*
[1]Bruker Nano Surfaces and Metrology, Nanoindentation Division, Eden Prairie, MN, USA

Silicon is a foundational material for modern microelectronics. As a semimetal, it exhibits complex and highly distinctive deformation behavior that depends on factors such as temperature, length scale, and stress state. These variables can activate a diverse set of deformation mechanisms, including brittle fracture, phase transformations, and dislocation-mediated plasticity. Understanding the onset of plasticity is valuable not only from a fundamental scientific perspective but also for practical applications, including semiconductor device reliability and the use of controlled strain to engineer electronic band structures.

This presentation will examine the broad spectrum of silicon deformation phenomena through a variety of *in situ* SEM and TEM experiments. Topics include brittle fracture investigated by double-cantilever micropillar splitting [1], room-temperature plasticity revealed through nanoparticle compression [2], and high-temperature plasticity and crack-tip shielding in doubly clamped bending beams [3]. *In situ* TEM nanoparticle compression offers insight into dislocation nucleation at stresses approaching the theoretical strength of defect-free silicon. These dislocations nucleate as partials and rapidly terminate at the opposite particle surface. For high-temperature crack-tip shielding, the effectiveness of shielding is assessed through post-mortem analysis of the observed dislocation arrays and corresponding estimates of shielding strength.

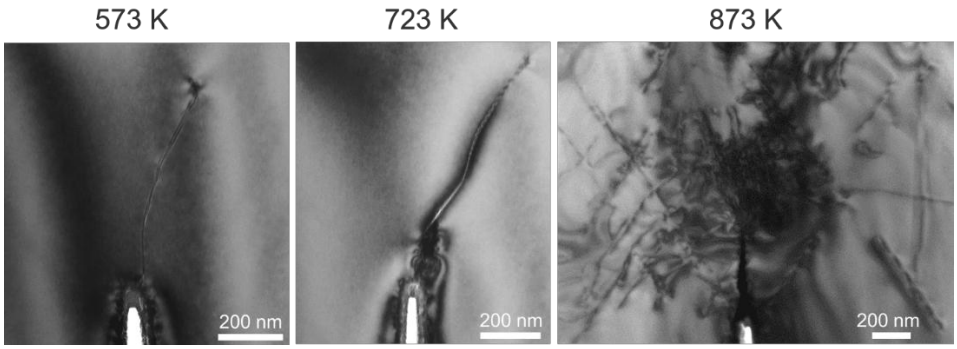
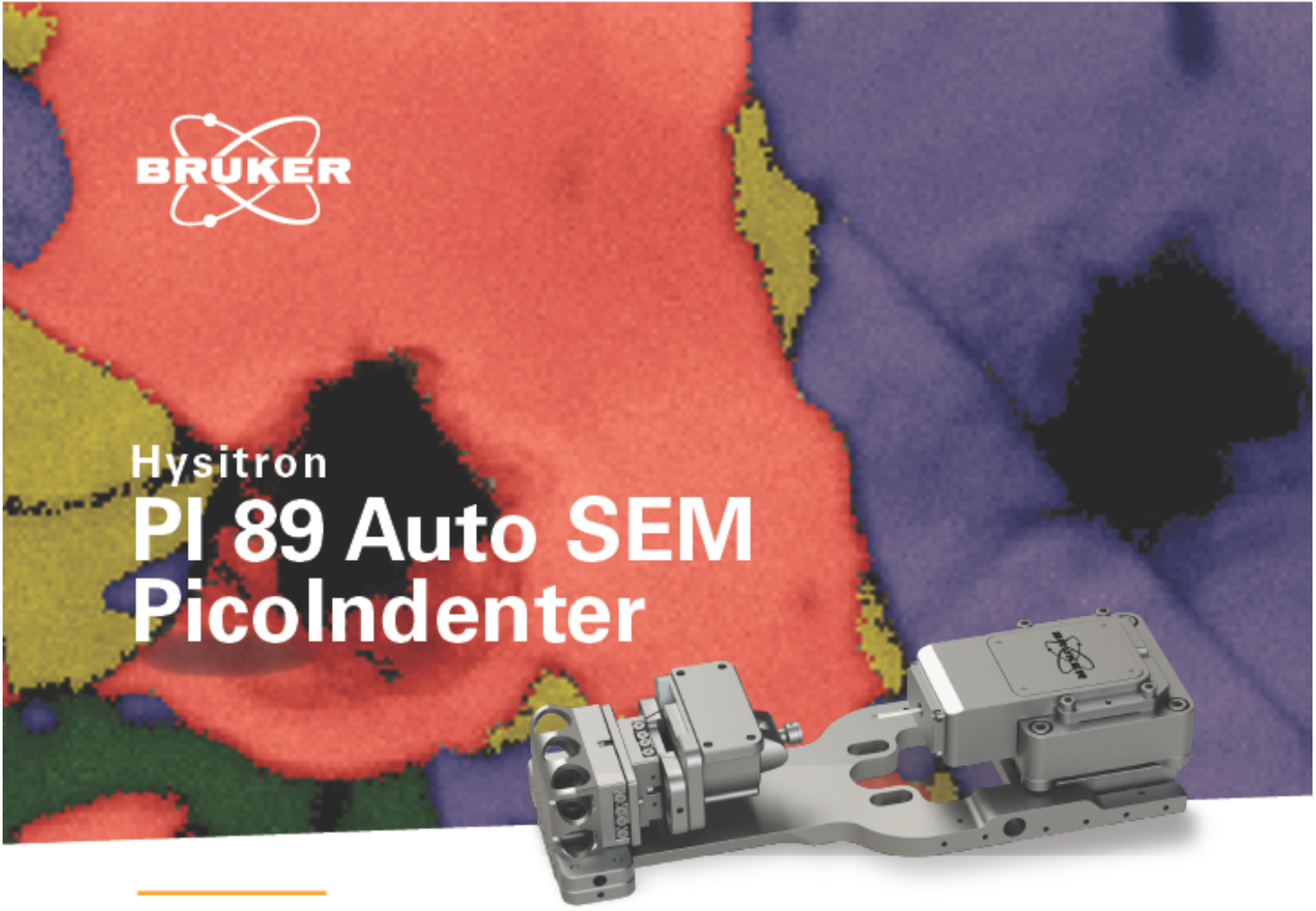


Fig. 1. Cracks extending from pre-notches in Silicon microbeams tested at different temperatures

References:

1. DelRio, F.W., Grutzik, S.J., Mook, W.M., Dickens, S.M., Kotula, P.G., Hintsala, E.D., Stauffer, D.D. and Boyce, B.L., 2022. Eliciting stable nanoscale fracture in single-crystal silicon. *Materials Research Letters*, *10*(11), pp.728-735.
2. Wagner, A.J., Hintsala, E.D., Kumar, P., Gerberich, W.W. and Mkhoyan, K.A., 2015. Mechanisms of plasticity in near-theoretical strength sub-100 nm Si nanocubes. *Acta Materialia*, *100*, pp.256-265.
3. Hintsala, E.D., Bhowmick, S., Yueyue, X., Ballarini, R., Asif, S.S. and Gerberich, W.W., 2017. Temperature dependent fracture initiation in microscale silicon. *Scripta Materialia*, *130*, pp.78-82.



BRUKER

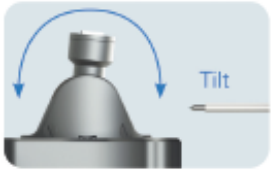
Hysitron

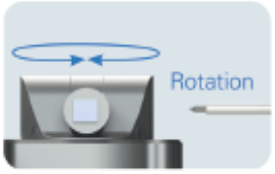
PI 89 Auto SEM PicoIndenter

Automated co-localized imaging and analysis for high-throughput in-situ nanoindentation

Automating Correlative Structure-Property Analysis

- Seamless switching between nanoindentation, standard SEM imaging, EBSD/EDS analysis
- Co-localized acquisition of quantitative in-situ mechanical data at user-defined regions of interest from imaging and analytical mapping
- Increased throughput without compromising precision or accuracy
- Automatic movement of the advanced rotation and tilt stage to the indentation position simplifies testing and analysis





The PI 89 Auto includes patented 5-axis (X, Y, Z, tilt, rotation) sample-positioning stage.

For more information please visit www.bruker.com

Innovation with Integrity

Thermo Fisher Scientific

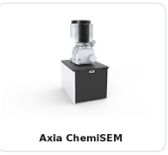
Materials & Structural Analysis

Helping customers make the world healthier, cleaner and safer.

Thermo Scientific solutions combine instrumentation, software and applications expertise to reveal material structure, chemistry and performance across scales.

SEM

Thermo Scientific SEM platforms combine high-resolution imaging, live elemental mapping, low-vacuum / ESEM flexibility and automation for routine to advanced materials analysis.


Axia ChemiSEM

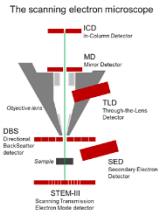

Quattro


Apreo 2 / ChemiSEM


Verios

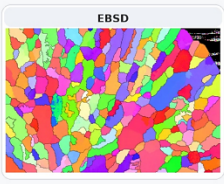
Solution strengths

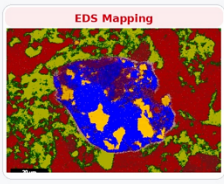
- Integrated SEM imaging and chemical characterization
- Live quantitative elemental mapping; EDS-ready workflows
- Sub-nanometer resolution options across broad kV ranges
- Low-vacuum / ESEM for wet, dirty or outgassing samples
- 3D serial block-face and compact desktop options



Application focus







DualBeam

Thermo Scientific DualBeam FIB-SEM platforms unite preparation, imaging, milling and automation to enable cross-sectioning, S/TEM prep, nanoprototyping and 3D analysis.


Scios 2 & 3


Helios FIB

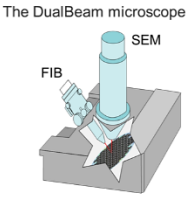

Helios PFIB


Helios Hydra

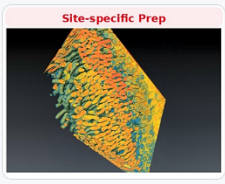

Helios TriBeam

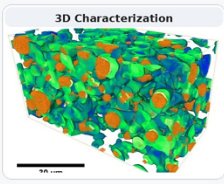
Solution strengths

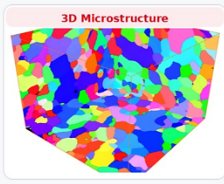
- Automated, high-quality S/TEM sample preparation
- High-throughput subsurface and 3D characterization
- Fast milling: plasma FIB, laser PFIB and high ion current
- Ga-free and multi-ion workflows for broad material compatibility
- Rapid nanoprototyping and advanced ease-of-use automation



Application focus







TEM

Thermo Scientific TEM/STEM platforms deliver atomic-scale imaging, spectroscopy and high-throughput analytical workflows for advanced materials research.

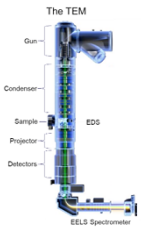

Talos Series


Spectra


Iliad

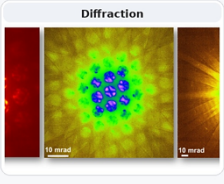
Solution strengths

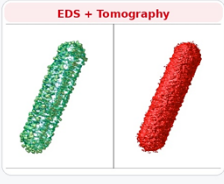
- Atomic-level structural and chemical information
- High-resolution TEM/STEM across 120-300 kV platforms
- EDS/EDX, EELS, diffraction and tomography capabilities
- High-throughput workflows with simultaneous multi-signal acquisition
- Automation and software for accurate, repeatable results



Application focus







XPS

Thermo Scientific X-ray photoelectron spectrometer (XPS) systems deliver surface-sensitive chemical-state analysis, imaging, depth profiling and multi-technique workflows.


K-Alpha

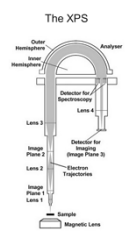

Nexsa


Hypulse

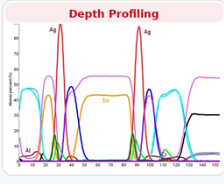

ESCALAB Xi+

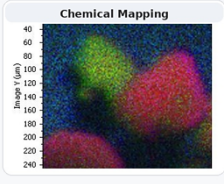
Solution strengths

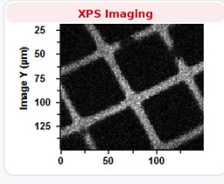
- High-resolution XPS for chemical-state surface analysis
- Fast automated workflows with ion-source depth profiling
- Multi-technique surface analysis and flexible sample prep
- Micro-focus X-ray sources for targeted analysis and imaging
- Dual-mode ion source for monoatomic and cluster profiling



Application focus







h-bar instruments

Featured in nature

"This super-cold microscope could spur a quantum revolution."

Isabel Gil, 22 Sept. 2026

LIQUID HELIUM CRYOGENIC TEM BELOW 1Å

We do supercool things.

h-Bar Instruments develops side-entry liquid helium cooling stages for next-generation cryogenic TEM: high-resolution imaging at ultracold sample temperatures, extended hold times, low stage drift, stable operation down to 20 K, and variable temperature control.

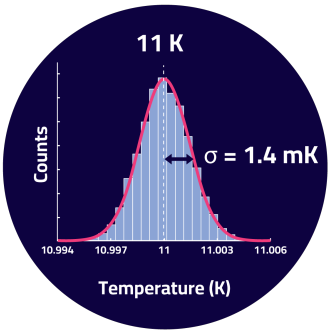
Atomic imaging with liquid helium cooling

TEM below 1Å
information transfer at ~20K

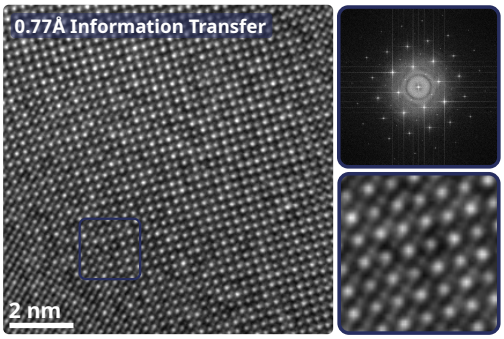
20 K
base temperature

±2 mK
thermal stability

10+ hours
hold times



High temperature stability



Atomic resolution of $SrTiO_3$ membrane at 40K

Manuscripts

ARXIV 2025

Liquid Helium Cryogenic TEM below 1 Å

Sub-angstrom atomic imaging at ultracold sample temperatures.

S.H. SUNG, ET AL. ARXIV (2025).
DOI: 10.48550/ARXIV.2509.12475

NATURE 2026

Imaging of nanoscale polar textures in quantum paraelectric $SrTiO_3$

Liquid helium cryogenic STEM down to 20 K directly images nanoscale polar textures in quantum paraelectric $SrTiO_3$.

Y. ZHANG, ET AL. NATURE (2026).
DOI: 10.1038/S41586-026-10823-X

PNAS 2025

Ultracold cryogenic TEM with liquid helium and high stability

Advances in mechanical and thermal stability of liquid helium holder enable atomic resolution TEM over multiple days.

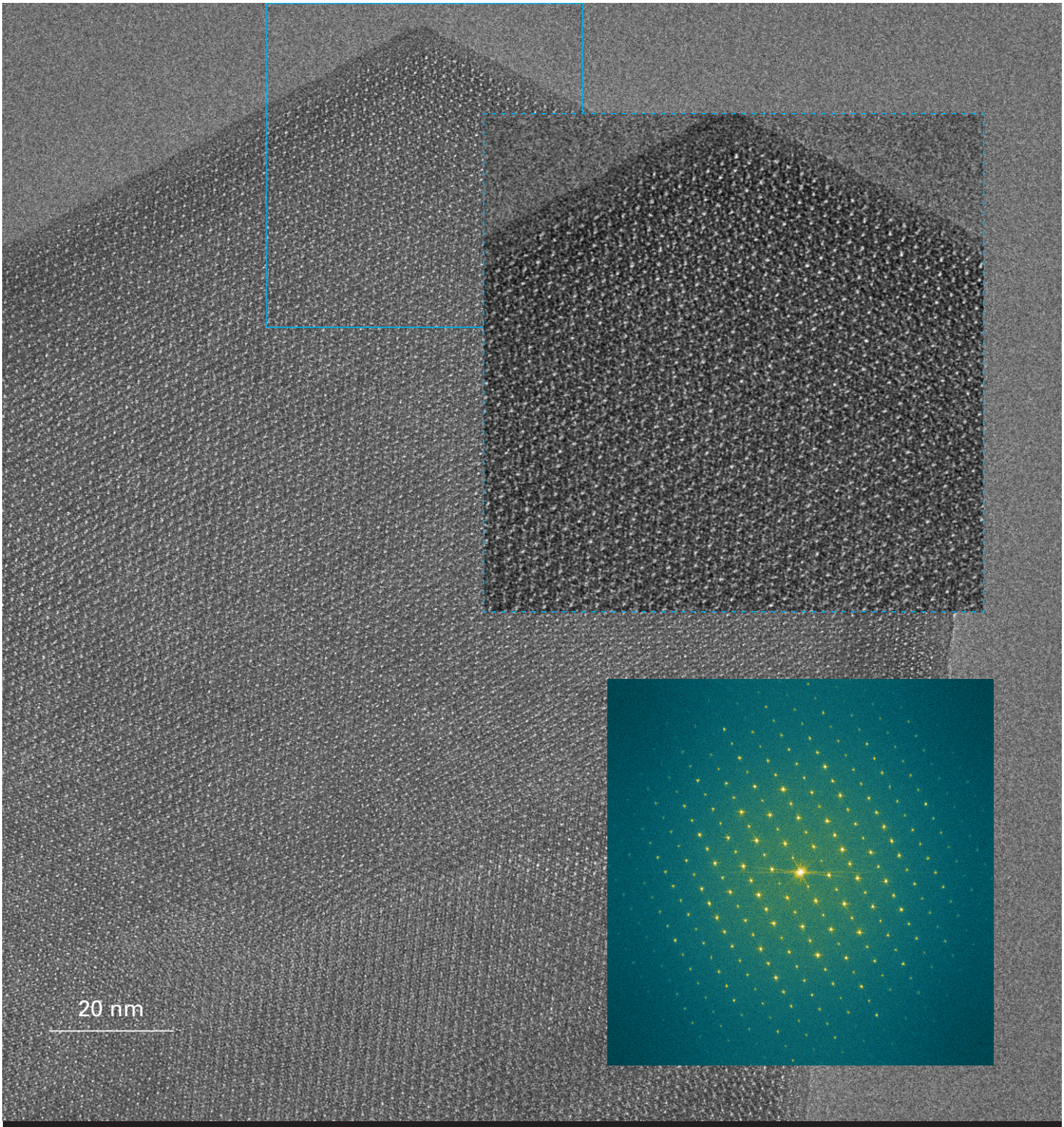
E. RENNICH, ET AL., PNAS, (2025).
DOI: 0.1073/PNAS.2509736122

MICROSC. AND MICROANAL. 2026

Helium-Cooled Cryogenic STEM Imaging and Ptychography for Atomic-Scale Study of Low-Temperature Phases

Liquid helium atomic-scale STEM and ptychography for probing low-temperature phases.

N. SCHNITZER, M. PALOS, ET AL. MICROSC. AND MICROANAL., (2026).
DOI: 10.1093/MAM/OZAG081



Counting for ≤200 kV

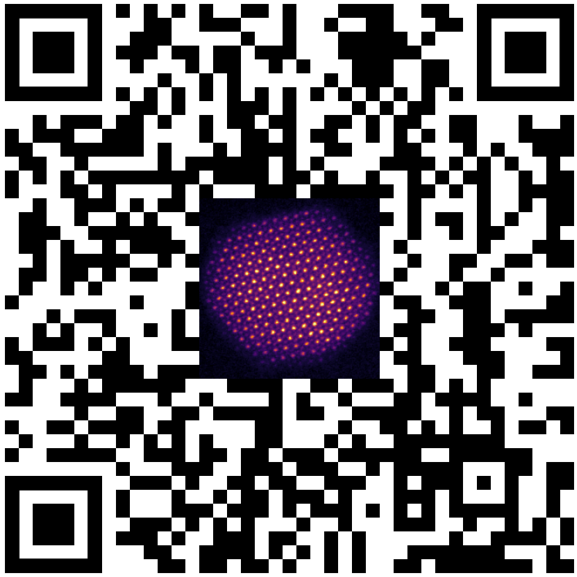
Metro® – The cutting-edge counting camera for groundbreaking imaging, diffraction, and in-situ studies. By enabling counting capabilities while operating your transmission electron microscope at low accelerating voltages (60 – 200 kV), imaging your most sensitive samples and low-dose studies is now within reach. This not only enhances results but allows you to push the research boundaries for 2D materials, batteries, catalysts, nanotubes, polymers, and organic/biological materials.

gatan.com

GATAN
AMETEK

Posters

Scan this QR code to make your vote to the fan-favorite poster awards!



https://greatlakes.microscopy.org/Fan-favorite-poster

Cy5-PEG4 Enables Blood–Brain Barrier-Penetrant Imaging of Mitochondrial Dynamics in Neuronal Systems

Muhammad Bilal Umar[1, 2], Zhiying Shan[2, 3] and Lanrong Bi[1, 2,]*
[1]Department of Chemistry, Michigan Technological University, Houghton, Michigan 49931
[2]Health Research Institute, Michigan Technological University, Houghton, Michigan 49931
[3]Department of Kinesiology and Integrative Physiology, Michigan Technological University, Houghton, Michigan 49931

Mitochondrial dysfunction is an early feature of many neurodegenerative disorders and is closely associated with altered mitochondrial morphology, distribution, and function. However, real-time visualization of mitochondria in the brain remains challenging because many conventional mitochondrial dyes exhibit limited tissue penetration, phototoxicity, and poor blood–brain barrier (BBB) permeability. Here, we introduce **Cy5-PEG4**, a near-infrared mitochondrial-targeting fluorescent probe designed for high-resolution imaging of mitochondrial dynamics in neuronal systems.

Cy5-PEG4 demonstrated efficient mitochondrial labeling in primary neuronal cells and enabled visualization of stress-induced, dose-dependent changes in mitochondrial morphology and organization. Its long-wavelength fluorescence provided strong imaging contrast while supporting observation of mitochondrial structural changes with reduced interference from cellular autofluorescence. Importantly, Cy5-PEG4 crossed the BBB following systemic administration and produced detectable mitochondrial-associated fluorescence in the brain without evidence of significant neuroinflammation or toxicity, supporting its application for non-invasive *in vivo* imaging.

The probe was further evaluated in three-dimensional neuronal culture models, where it enabled visualization of dynamic changes in mitochondrial distribution, morphology, and spatial organization during cellular maturation. These 3D imaging studies demonstrate the ability of Cy5-PEG4 to resolve mitochondrial remodeling within complex cellular architectures that more closely resemble native tissue environments.

Together, these findings establish Cy5-PEG4 as a versatile mitochondrial imaging platform spanning conventional cell microscopy, three-dimensional culture imaging, and *in vivo* brain visualization. Its combination of mitochondrial targeting, long-wavelength fluorescence, BBB permeability, and compatibility with multidimensional imaging provides a promising approach for studying mitochondrial dynamics, detecting early mitochondrial dysfunction, and evaluating therapeutic responses in neurological disease.

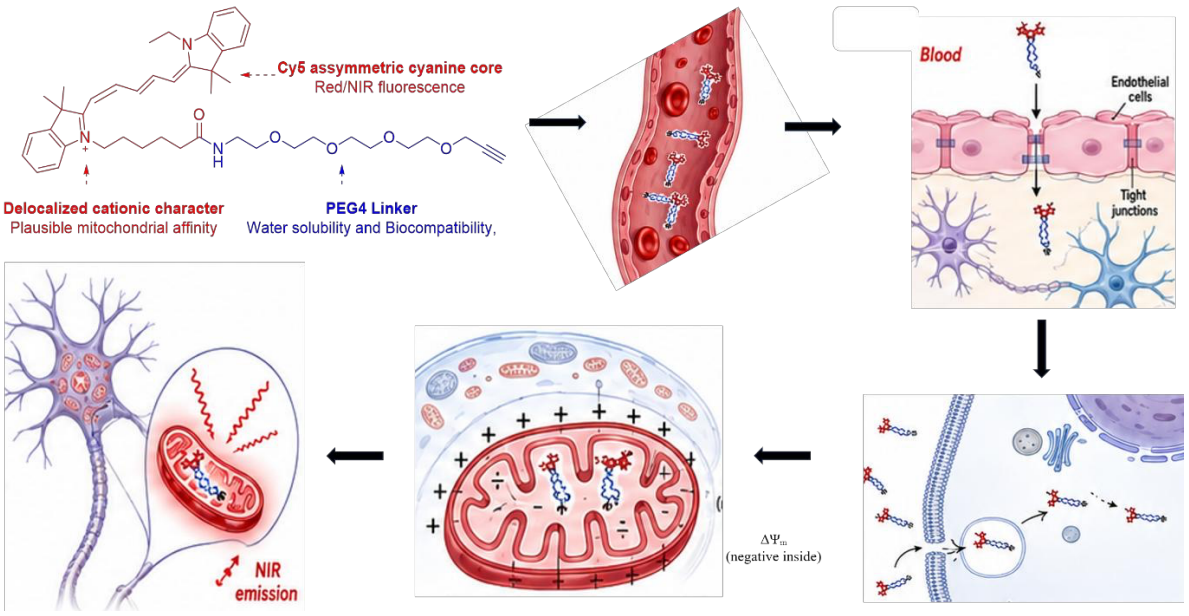


Fig. 1. Proposed Mechanism of Cy5-PEG4 for Mitochondrial and Brain Imaging.

Real-Time Visualization of Mitophagy Flux by Reversible Mitochondrial Redox Fluorescence Imaging

*Brayden Storey, Lanrong Bi**

Department of Chemistry, Michigan Technological University, Houghton, Michigan 49931

Mitophagy is a dynamic mitochondrial quality-control process that requires coordinated changes in mitochondrial redox state, organelle trafficking, lysosomal engagement, and cargo degradation. However, conventional fluorescence approaches often provide only static snapshots or rely on irreversible reactive oxygen species (ROS) probes, limiting their ability to resolve the temporal progression of mitophagy in living cells. To address this imaging challenge, we developed MitoFlare, a mitochondria-targeted, reversible redox-responsive fluorescent probe for continuous visualization of mitochondrial oxidative dynamics during mitophagic flux.

MitoFlare incorporates two TEMPO nitroxide quenchers into a long-wavelength rhodamine fluorophore, producing >95% suppression of basal fluorescence followed by rapid fluorescence activation in response to mitochondrial oxidative species. Importantly, the fluorescence response is reversible, allowing repeated visualization of changes in mitochondrial redox activity within the same living cell rather than providing a cumulative record of oxidation. Combined with LysoTracker Green, MitoFlare enables dual-channel live-cell fluorescence microscopy that simultaneously tracks mitochondrial redox activation and mitochondrial-lysosomal interactions with high spatial and temporal resolution.

Using this imaging platform in neuronal cells, we resolved distinct stages of mitophagy, including early redox activation and mitochondrial-lysosomal recruitment, intermediate organelle colocalization and fusion, and terminal lysosomal processing. Nutrient deprivation produced a coordinated temporal sequence characterized by increased mitochondrial redox signaling, progressive mitochondrial–lysosomal association, and subsequent clearance of mitochondrial cargo. In contrast, inhibition of lysosomal acidification with bafilomycin A1 disrupted the terminal processing stage and resulted in persistent mitochondrial-lysosomal structures containing redox-active mitochondrial material. These intermediates were readily visualized through the reversible fluorescence response of MitoFlare, revealing dynamic features that are difficult to distinguish using conventional irreversible ROS probes.

Together, these results demonstrate that reversible mitochondrial redox imaging can be integrated with organelle-specific fluorescence microscopy to directly visualize mitophagic flux in living cells. The approach transforms mitophagy analysis from endpoint colocalization measurements into a time-resolved imaging strategy capable of following mitochondrial oxidative activation, organelle interaction, and lysosomal processing within the same experimental system. MitoFlare therefore provides a versatile microscopy platform for investigating mitochondrial quality control and for identifying stage-specific defects in mitophagy under physiological and pathological conditions.

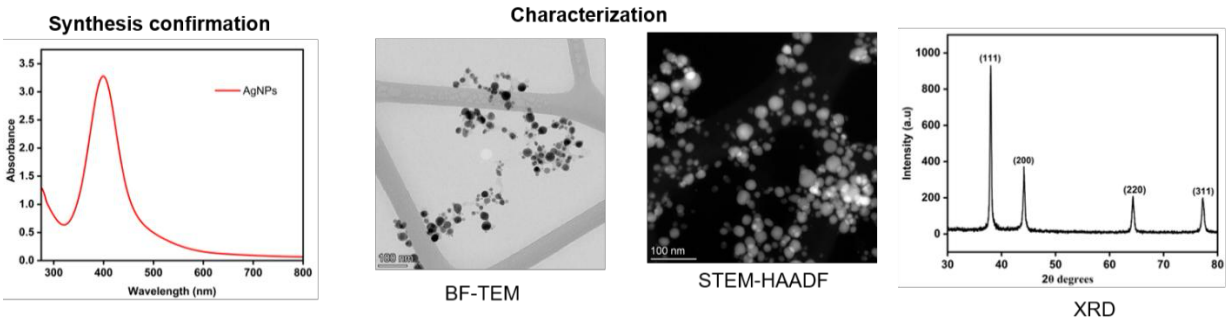
Multiscale Correlative Microscopy of Surface-Engineered Silver Nanoparticles: From Nanoscale Architecture to In Vitro and In Vivo Label-Free Bio-Tracking

Jije Geyesa[1], Ashlyn Beatty[2], Micaela Geborkoff[2], Madeleine Roux[2], Emma Enot[2], Athar Ata[1], Thomas Werner[2] and Lanrong Bi[1]*

[1]Department of Chemistry, Michigan Technological University, Houghton, MI, USA

[2]Department of Biological Sciences, Michigan Technological University, Houghton, MI, USA

Bio-derived nanomaterials often vary widely in size and surface properties because crude natural extracts are complex and inconsistent. In this study, we used a multiscale microscopy workflow to characterize silver nanoparticles stabilized by a single, defined natural capping molecule. Using transmission electron microscopy (TEM), we directly imaged the particles' internal crystal defects and dense silver cores, which ranged from 6 to 40 nm. Powder X-ray diffraction (XRD) confirmed that the particles consist of pure, crystalline metallic silver, while infrared spectroscopy (FTIR) showed that the natural coating binds tightly to the metal surface. These physical measurements matched solution-state particle sizes measured by nanoparticle tracking analysis (NTA). Notably, Fluorescence spectroscopy coupled with computer simulations revealed that electron movement between the surface coating and the silver core, termed ligand-to-metal charge transfer (LMCT), generates intrinsic fluorescence directly from the particles. This built-in emission eliminates the need for chemical dye tags, which can alter particle size, charge, and biological behavior. Leveraging this intrinsic fluorescence, live-cell confocal microscopy in HeLa cells showed particles entering cells and colocalizing with specific metabolic and waste-processing compartments without cell fixation. Extending this label-free imaging in vivo, we evaluated concentration-dependent ingestion and systemic uptake in living *Drosophila melanogaster* larvae, quantifying whole-organism fluorescence distribution across regions of interest. Overall, this combined imaging approach shows how standard electron microscopy and optical bio-tracking can be utilized to evaluate functional nanomaterials from single nanometer crystals to living organisms.



Graphical abstract

Specific Protein Nanoparticle Crosslinking for Protein Delivery

Kate Kaplin[1,2], Michael Triebwasser[1], and Joerg Lahann[1,3]*

[1]University of Michigan, Biointerfaces Institute, Ann Arbor, MI, United States

[2]University of Michigan, Department of Chemistry, Ann Arbor, MI, United States

[3]University of Michigan, Department of Chemical Engineering, Ann Arbor, MI, United States

Prior work in the Lahann Lab has focused on the capabilities of electrohydrodynamic (EHD) jetted synthetic protein nanoparticles (SPNPs) to cross the blood brain barrier (BBB) and treat glioblastoma in mice1. In addition to crossing the BBB, these EHD jetted SPNP have advantages over lipid nanoparticles such as greater bioavailability and a longer circulation time. The stability of these particles is due to a homobifunctional polyethylene glycol (PEG) linker which is added to the jetting solution and covalently binds to the lysine amino acid of proteins. As lysine is among the most common amino acid residue in proteins, this ubiquitous protein crosslinking poses a challenge to the delivery of protein-based therapeutics via SPNP. Therefore, to enhance the versatility of SPNPs and allow for the encapsulation and release of protein therapeutics we have harnessed click chemistry to selectively crosslink proteins in the SPNPs – only crosslinking the structural protein of the SPNP and leaving the therapeutic compound unlinked (figure 1). By functionalizing human serum albumin (HSA) with a dibenzocyclooctyne (DBCO) moiety and crosslinking with a homobifunctional azido polyethylene glycol (PEG) linker, we are able to specifically crosslink the HSA without concern of side reactivities with therapeutic protein compounds. This particle system also shortens the fabrication timeline and vastly improves the yield when compared to standard EHD Jetting SPNP formulations. *In vitro c*argo release studies of fluorescent protein Allophycocyanin (APC) demonstrate the therapeutic capabilities of this specific crosslinking method while providing information to the release kinetics from the material (figure 2).

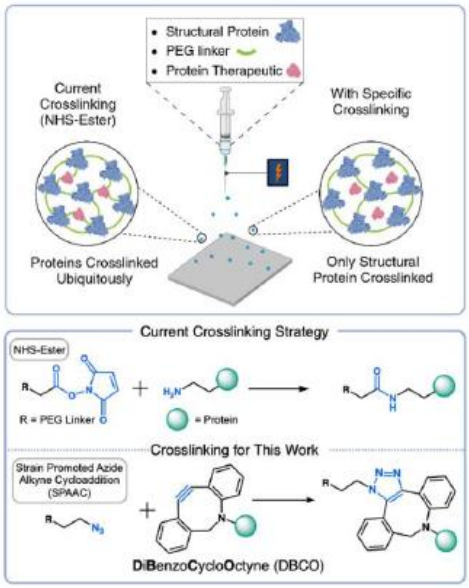


Figure 1: Strategy for the preparation of specific crosslinking synthetic protein nanoparticles using strain promoted azide alkyne click chemistry (SPAAC)

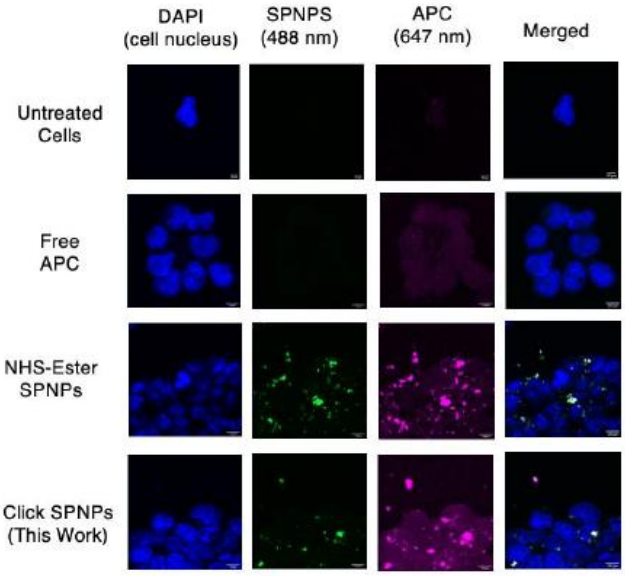


Figure 2: Confocal imaging of fixed HEK293 cells after 48hr incubation with varying cargo: Empty, Free APC, APC loaded NHS-Ester SPNPs, and APC loaded Click SPNPs,

References:

1. Gregory, J. V.; Kadiyala, P.; Lahann, J. *Nature Communications* **2020**, *11* (1), 5687.

Microscopic Characterization and In Vivo Vascular Response of Polydopamine-Cu(II)-Coated Biodegradable Zinc

Md Tanvir Hossain[1], J. Goldman[2], J. W. Drelich[1,]*

[1]Department of Materials Science and Engineering, Michigan Technological University, Houghton, MI, 49931, USA

[2]Department of Biomedical Engineering, Michigan Technological University, Houghton, MI, 49931, USA

Zinc (Zn) has emerged as a promising biodegradable metal for temporary vascular implants because of its physiological relevance and favorable behavior in vascular environments. However, achieving a favorable implant-tissue interface while minimizing excessive neointimal formation remains an important challenge for Zn-based vascular devices. Surface functionalization offers an attractive approach for modifying the biological interface without changing the bulk properties of the underlying Zn. Among available surface modifiers, polydopamine (PDA) is particularly attractive because of its mussel-inspired adhesive chemistry, straightforward aqueous deposition, and ability to form conformal coatings on diverse substrates. Its catechol- and amine-rich chemistry provides abundant functional groups for surface interactions and coordination with metal ions and may also influence protein adsorption and subsequent cellular responses at the implant interface. Incorporation of Cu(II) into PDA provides an additional biofunctional component. Cu is a biologically relevant trace element, and Cu-containing surfaces have been investigated for their potential to support vascular functions, including endothelial responses and catalytic generation of nitric oxide (NO) from endogenous S-nitrosothiols. Therefore, integrating Cu with PDA provides a potentially multifunctional interface for biodegradable vascular implants. In this study, PDA and Cu(II)-incorporated PDA (PDA-Cu) coatings were developed on high-purity Zn wires, and complementary electron microscopy, elemental microanalysis, and histological microscopy were employed to investigate coating morphology, Cu distribution, and the subsequent in vivo vascular response.

High-purity Zn wires (>99.99%, 0.25 mm diameter) were used as substrates. PDA coatings were prepared using 0.25 g/L dopamine hydrochloride in 10 mM Tris-HCl buffer (pH 8.5), while PDA-Cu coatings were prepared by incorporating $CuCl_2$ at concentrations of 5, 10, and 20 mg/L. For nanoscale characterization, dopamine-Cu precursor solutions were drop-cast onto ultrathin lacey carbon-coated Au TEM grids (300 mesh), dried under ambient conditions for 24 h, and analyzed using an aberration-corrected FEI Titan Themis operated at 200 kV. Transmission electron microscopy (TEM) revealed nearly spherical PDA-Cu5 particles with an average diameter of 120 ± 30 nm, determined from measurements of 160 particles (Figure 1). High-angle annular dark-field scanning

transmission electron microscopy (HAADF-STEM), combined with energy-dispersive X-ray spectroscopy (EDS), confirmed the presence of C, N, O, and Cu. STEM-EDS elemental mapping further demonstrated a homogeneous distribution of Cu throughout the PDA particles without detectable Cu-rich agglomeration. These observations demonstrate successful incorporation of Cu within the nanoscale PDA architecture and provide direct microscopic evidence of the structural and compositional characteristics of the functional coating.

For in vivo evaluation, bare Zn and PDA-Cu5-coated Zn wires were implanted into rat abdominal aortas following a protocol approved by the Michigan Technological University Institutional Animal Care and Use Committee (IACUC). After 4 months of implantation, arterial specimens containing the wires were collected, embedded in optimum cutting temperature (OCT) compound, snap-frozen, and cryosectioned. We performed Verhoeff-Van Gieson (VVG) staining to visualize vascular architecture and distinguish elastic laminae from surrounding neointimal tissue. VVG-stained cross-sections were imaged at 20× magnification using a Zeiss Axioscan Z1 digital slide scanner. Quantitative histomorphometric measurements were performed on three specimens using Olympus cellSens Dimension software (Version 2.3). Wire-to-lumen thickness (WLT), base neointimal length (BNL), and neointimal area (NA) were quantified to evaluate tissue formation surrounding the implanted wires. VVG microscopy revealed marked differences in the vascular tissue response surrounding bare and surface-modified Zn implants (Figure 2). Bare Zn exhibited greater neointimal development and less favorable preservation of the local arterial architecture, whereas PDA-Cu5-coated Zn showed a thinner and more uniform neointimal region with better-preserved vascular structure. Quantitative histomorphometry supported the microscopic observations, showing reductions of approximately 55% in BNL, 59% in WLT, and 67% in NA for the surface-modified implants relative to bare Zn.TEM, HAADF-STEM/EDS, and VVG microscopy linked the coating characteristics with the subsequent vascular tissue response. The reduced neointimal formation supports PDA-Cu functionalization as a promising surface-engineering strategy for biodegradable Zn vascular implants.

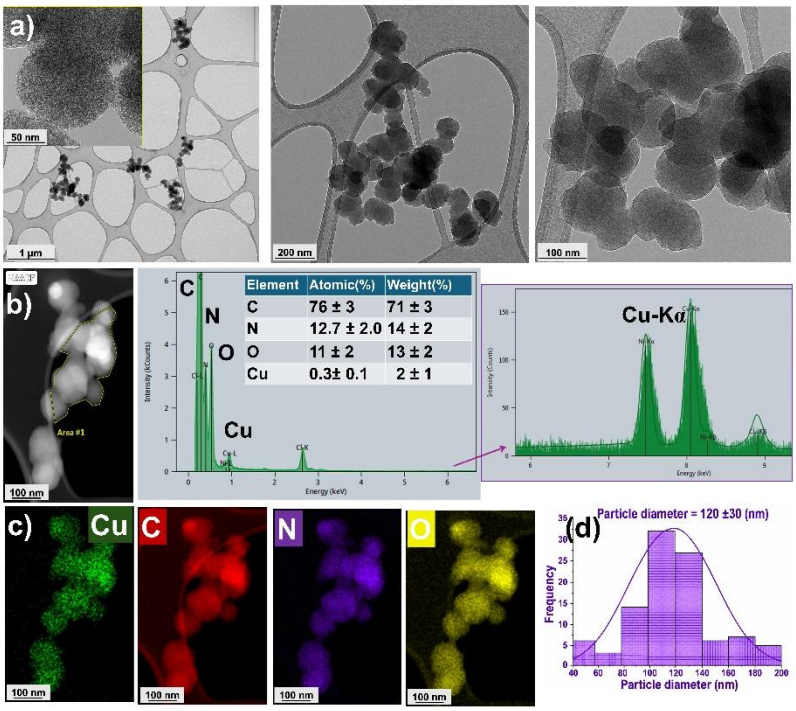


Fig. 1. Morphological and elemental characterization of PDA-Cu particles. (a) TEM images of spherical PDA-Cu5 particles with a mean diameter of 120 ± 30 nm. (b) HAADF-STEM image and EDS spectrum confirming Cu incorporation. (c) STEM-EDS elemental maps of Cu, C, N, and O showing homogeneous Cu distribution within the PDA particles.

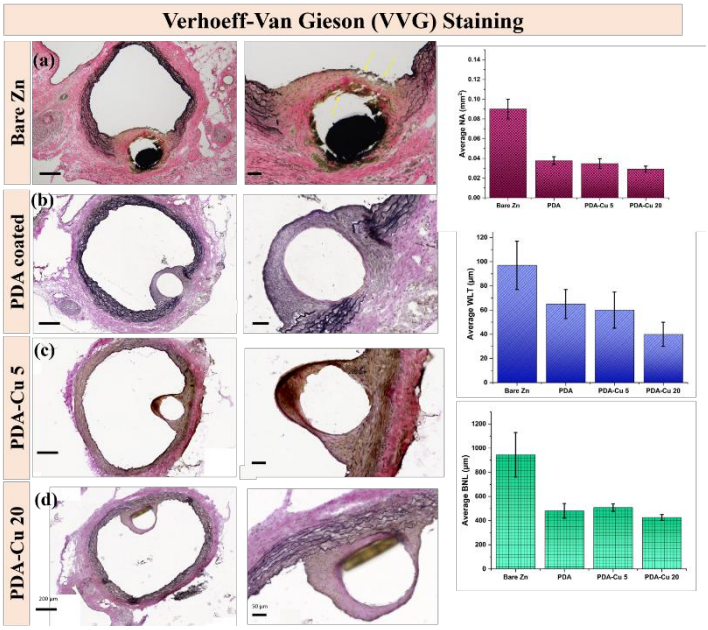


Fig. 2. Verhoeff-Van Gieson (VVG)-stained cross-sections of rat abdominal arteries after 4 months of implantation with (a) bare Zn, (b) PDA-coated Zn, (c) PDA-Cu5-coated Zn, and (d) PDA-Cu20-coated Zn wires. Representative low- and high-magnification images are shown together with quantitative histomorphometric analysis of neointimal area (NA), wire-to-lumen thickness (WLT), and base neointima length (BNL).

A Novel Method to Vascularize Organoids Using Microfluidic Devices

*Viviana Secci[1,2,3,4], Ylliah Jin[5], Zhengpeng Wan[*4,5,6,7]*

[1] Department of Chemistry, Materials and Chemical Engineering "Giulio Natta", Politecnico di Milano, Milan, Italy.

[2] Regenerative Medicine Division, Institute for Translational Research, Ente Ospedaliero Cantonale - Università della Svizzera Italiana, Bellinzona, Switzerland.

[3] Euler Institute Biomedical Sciences Faculty, Università della Svizzera Italiana (USI), Lugano, Switzerland.

[4] Department of Biomedical Engineering, Michigan Technological University, Houghton, MI.

[5] Department of Biological Engineering, Massachusetts Institute of Technology, Cambridge, MA, 02139, USA.

[6] Department of Mechanical Engineering, Massachusetts Institute of Technology, Cambridge, MA, 02139, USA.

[7] Health Research Institute, Michigan Technological University, Houghton, MI, USA.

Organoids hold great appeal for drug testing and personalized medicine, particularly for heterogeneous conditions like cancer. However, current models are limited by a lack of vascularization, which causes central necrosis and reduces physiological relevance. To overcome this limitation, we developed a microfluidic approach to create a pre-formed vascular network within a tumor microenvironment (TME) that anastomoses with an external healthy vascular network. Endothelial cells (iPSC-derived ECs or immortalized HUVECs), fibroblasts , and tumor or organ-specific cells were co-cultured for 7 days in custom polydimethylsiloxane (PDMS) "butterfly" devices to establish a vascular network. Perfusability of the resulting microvascular network (MVN) was confirmed via confocal microscopy using fluorescent dextran. The vascularized constructs were then retrieved, transferred to low-adhesion plates, and allowed to condense into vascularized spheroids over 2 days. Each spheroid was subsequently embedded in a single-channel microfluidic device alongside additional ECs and fibroblasts to induce functional anastomosis between internal and external vascular networks. Optimizing tumor cell density in the initial stage was critical to maintaining a functional MVN throughout the 14-day culture period. This adaptable platform successfully integrates organ-specific or pathological MVNs with healthy vascular networks, offering a versatile tool for modeling tissue vascularization, tumor–immune interactions, and high-throughput drug screening.

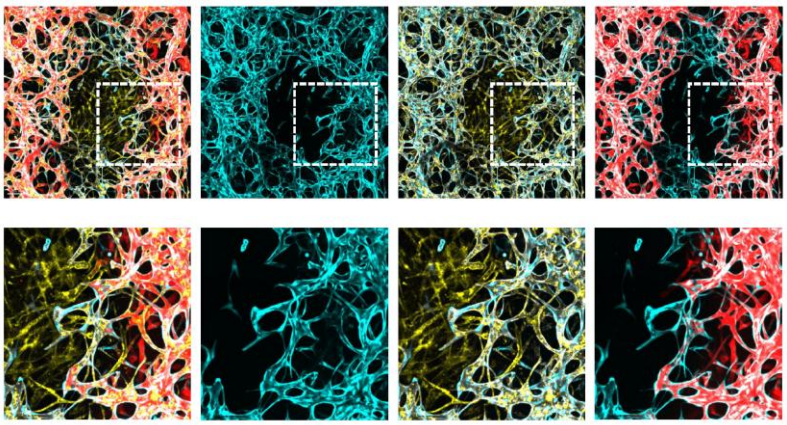


Figure 1. ImHUVEC-BFP anastomose to iPSCs-EC from spheroid forming perfusable MVNs. Representative images of MVNs formed by outer-layer ImHUVEC expressing blue fluorescent protein (BFP) and induced pluripotent stem cell derived endothelial cells (iPSC-EC) MVN from the vascularized spheroid. Perfusion is demonstrated using dextran (10 kDa, red). Endothelial cells stained with UEA-I,yellow.

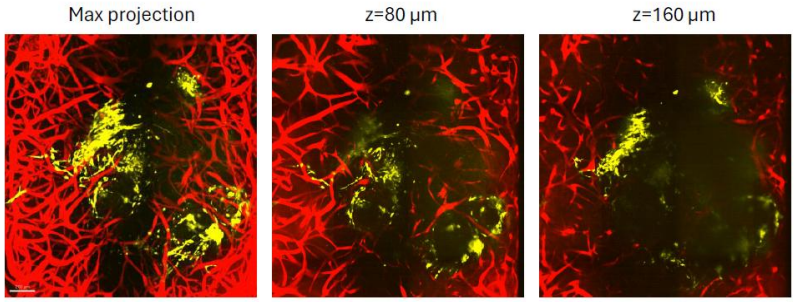


Figure 2. iPSCs-EC external vasculature connected with vascularized tumor MVN.

Representative images of tumor spheroid MVNs connected to external iPSC-EC MVN. Cancer cells (SKOV-3) in yellow. Perfusion is demonstrated using dextran (10 kDa, red).

MitoGlow-ROS Enables High-Dynamic-Range, Multi-Scale Fluorescence Imaging of Mitochondrial Oxidative Stress from Cells to Brain Tissue

Jake Williams[1], Zhiying Shan[2], and Lanrong Bi[1]*
[1]Michigan Technological University, Chemistry Department, Houghton, Michigan, USA
[2] Michigan Technological University, Biological Sciences Department, Houghton, Michigan, USA

Quantitative imaging of mitochondrial reactive oxygen species (mtROS) remains challenging because commonly used fluorescent probes may exhibit limited dynamic range, rapid signal saturation, and insufficient sensitivity to resolve subtle spatial and temporal differences in mitochondrial oxidative stress. Here, we establish MitoGlow-ROS as a high-sensitivity fluorescence imaging platform for quantitative visualization of mitochondrial superoxide across multiple biological scales, ranging from cell-free calibration systems to cultured cells, primary neurons, and intact brain tissue.

MitoGlow-ROS incorporates a dynamic fluorescence-quenching mechanism designed to expand the measurable response range and improve quantitative detection of mitochondrial superoxide. In a cell-free superoxide-generating system, the probe produced a 45-fold fluorescence dynamic range with strong linearity (R^2 = 0.97) and a detection limit of 0.05 μM/min, providing enhanced sensitivity and reproducibility compared with MitoSOX Red. These characteristics enabled visualization of both modest and pronounced changes in oxidative activity without rapid signal saturation.

We next evaluated the probe at the cellular level using fluorescence microscopy. In PC12 cells treated with the mitochondrial complex III inhibitor antimycin A, MitoGlow-ROS resolved a concentration-dependent increase in mitochondrial fluorescence of up to 5-fold above baseline. Pretreatment with N-acetylcysteine reduced the fluorescence response by approximately 80%, supporting ROS-dependent probe activation and demonstrating the ability of the imaging system to quantitatively track pharmacologically induced changes in mitochondrial oxidative state.

The platform was subsequently extended to time-resolved imaging in primary neuronal cultures exposed to lipopolysaccharide (LPS). Quantitative fluorescence analysis revealed a progressive mitochondrial ROS response culminating in a 3.4-fold signal increase at 6 h. This temporal imaging profile followed early activation of inflammatory and antioxidant pathways, including marked induction of IL-6 and SOD2, demonstrating the ability of MitoGlow-ROS imaging to connect dynamic mitochondrial redox changes with cellular stress responses.

Finally, MitoGlow-ROS was applied to an in vivo rat model of neuroinflammation to resolve region-specific mitochondrial oxidative stress within brain tissue. Fluorescence imaging revealed a pronounced 4.1-fold increase in hippocampal mtROS compared with a 2.8-fold increase in the cortex, demonstrating that the probe can distinguish anatomically heterogeneous oxidative responses that may be difficult to detect using bulk biochemical measurements.

Together, these studies demonstrate a multi-scale microscopy workflow for quantitative mtROS imaging, spanning controlled calibration, single-cell imaging, temporal neuronal analysis, and spatially resolved brain tissue measurements. The broad dynamic range, high sensitivity, and ability to resolve both temporal and regional heterogeneity establish MitoGlow-ROS as a promising fluorescence microscopy tool for visualizing mitochondrial redox biology and investigating spatially complex oxidative-stress responses in biological systems.

Anion-Directed Self-Assembly of Copper Iodide-Penicillamine Frameworks: Tuning Morphology and Chiroptical Properties

*Riva Akter[1,3,4], and Nicholas A. Kotov[*2,3,4]*

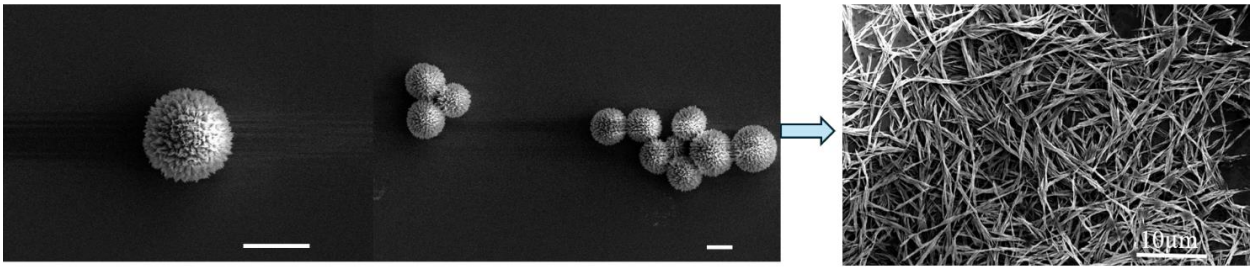
1Department of Chemistry, University of Michigan, Ann Arbor, MI, 48109, USA

2Department of Chemical Engineering, University of Michigan, Ann Arbor, MI, 48109, USA

3Biointerfaces Institute, University of Michigan, Ann Arbor, MI, 48198, USA

4Center for Complex Particle Systems (COMPASS), University of Michigan, Ann Arbor, MI, 48198, USA

Abstract: Designing anion receptors with high selectivity has remained a persistent and demanding challenge in supramolecular chemistry, largely due to their strong hydration, diffuse charge, and low interaction specificity. Extending their role from simple host-guest complexation to dynamic bridging that drives the hierarchical self-assembly of chiral metal-organic matter is even more demanding and remains largely unexplored. Here, we demonstrate that iodide and pseudohalides coordinate to copper-thiolate building blocks, forming labile coordination bridges that direct self-assembly into complex chiral superstructures. Through solvent-mediated anion exchange, the pre-assembled chiral supraparticles undergo driven phase transformations such as restructuring from hierarchical hedgehogs into highly crystalline 1D nanofibers, demonstrating extraordinary structural adaptability. Precise variation of anion identity and concentration, along with pH and temperature, provides orthogonal control over lattice parameters, morphology, and assembly states without compromising framework integrity. This dynamic anion exchange reorganizes the underlying inorganic lattice, directly modulating both circular dichroism and circularly polarized luminescence. These findings establish simple anions not merely as passive structural counterions, but as active, reversible chemical linkers that couple molecular recognition with emergent chirality and tunable photonic activity in adaptive metal-organic supraparticles.



Integrative Microscopy Delineates Biogenesis and Self-Assembly of Extracellular Matrix Polymers in Diatoms

Michael R. Gretz[1*]

[1]*Great Lakes Research Center, Michigan Technological University, Houghton, Michigan, USA*

The self-assembly process of extracellular matrix polymers (ECM) extruded through nanopores and slits in the silica “shoe box” frustule of diatoms (single celled algae) has been investigated using a combination of cryo-field emission SEM (cryo-FE-SEM), high pressure freezing/freeze substitution (HPF/FS-TEM), colloidal gold-EM immunocytochemistry, and video microscopy. Cryopreservation required due to the high level of hydration and fragility of the ECM polymers was accomplished through fast-freezing, freeze fracture, freeze sublimation, cryo-coating, cryotransfer and cryo-FESEM observation. High-resolution, time lapse video microscopy revealed that production of a highly organized ECM “stalk” was correlated with vesicle transport and deposition to a certain region of the plasma membrane underlying the major slit in the frustule, the raphe. TEM observations of the ECM preserved by HPF/FS showed detailed structure of mucilaginous polymers in vesicles and post-assembly. Cryo-FESEM and HPF/FS TEM demonstrated that secreted adhesives, appearing as fine fibrils, were passed through the diatotepum, a continuous, multi-layered intervening layer, located between the plasma membrane and the silicon frustule. These fine fibrils were then extruded through frustule slits and pores. Monoclonal antibody-colloidal gold conjugates labeled intracellular vesicles near the perinuclear Golgi apparatus, and differentiated fibrils secreted through the diatotepum and the raphe. Distinct and unique antibody labeling patterns appeared on the stalk during the self-assembly process external to the frustule where fibrillar materials were organized into four distinct layers of the m ature stalks, each with a unique chemistry.

Single-particle characterization of mechanical and surface properties of empty and full AAV9 Capsids using atomic force microscopy

Vaishali Sharma [1,2], Bianca Mercado Velez [2,3] Caryn L. Heldt [1,2]
[1] Department of Chemical Engineering, Michigan Technological University
[2] Health Research Institute, Michigan Technological University
[3] Department of Biological Sciences, Michigan Technological University

Adeno-associated virus (AAV) has emerged as an important platform for gene therapy because of its ability to deliver genetic material in vivo, with favorable tissue tropism and relatively low immunogenicity. After FDA approved 5 AAV-based therapies, the field continues to advance. Reducing the high cost of AAV-based therapies will increasingly depend on improving manufacturing efficiency and product quality. One major challenge in AAV manufacturing is separating full capsids from empty capsids, which conventional approaches struggle to distinguish [1]. Although differences in surface charge between empty and full capsids can be used for capsid enrichment by chromatography, this method typically does not provide a purity of full capsids above 80%. These changes may also vary across individual particles and therefore be difficult to capture with bulk measurements or high-resolution techniques that rely on averaging across many particles. In this study, we used atomic force microscopy (AFM) to investigate differences between empty and full AAV9 particles through nanoindentation and chemical force microscopy (CFM). Nanoindentation measurements showed that full AAV9 capsids were substantially stiffer than empty capsids. Using AFM probes functionalized with a positive charge, no substantial difference between empty and full particles was measured. However, hydrophobic probes revealed a clear difference in surface interactions. Because these measurements are performed at the single-particle level, AFM provides a broader view of heterogeneity within a virus population that bulk measurements may not capture. Together, these results show that genome packaging affects both the mechanical properties and surface characteristics of AAV9 and demonstrate the potential of single-particle AFM measurements to provide a more detailed understanding of AAV populations and the differences between empty and full capsids.

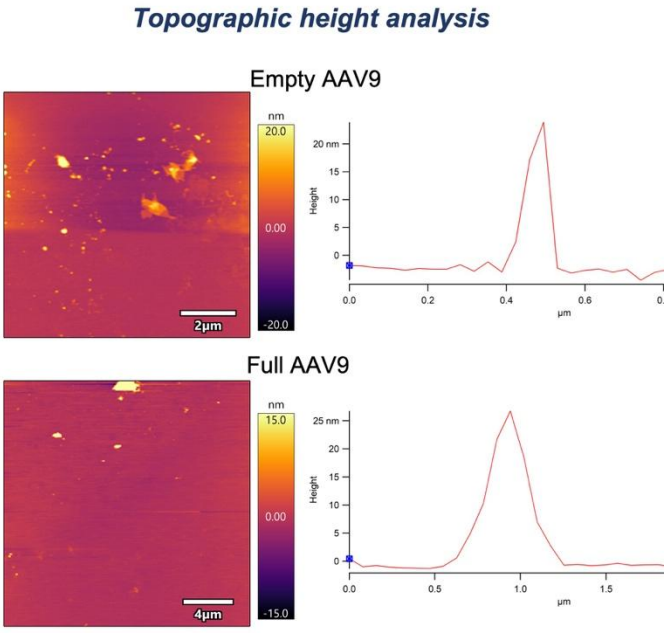


Fig. 1. Topographic height analysis of empty and full AAV9 capsids using AFM.

References:

1. Mingozzi, F. and K.A. High, *Therapeutic in vivo gene transfer for genetic disease using AAV: progress and challenges.* Nature reviews genetics, 2011. **12**(5): p. 341-355.

Measuring the Three-dimensional Coordinates of Atoms with Through Focal Electron Tomography

Eric M. Orson[1,2], Jonathan Schwartz[2,3], Suk Hyun Sung[2,4], Reed Yalisove[2,5], Peter Ercius[5], Sarah A. Lindley[6], Mary C. Scott[5,7], Colin Ophus[5,8], and Robert Hovden[1,2]*

[1]*Applied Physics Program, University of Michigan, Ann Arbor, MI.*
[2]*Department of Material Science and Engineering, University of Michigan, Ann Arbor, MI.*
[3]*Biohub, Redwood City, CA.*
[4]*Michigan Center for Materials Characterization, Ann Arbor, MI*
[5]*National Center for Electron Microscopy, Lawrence Berkeley National Laboratory, Berkeley, CA.*
[6]*Department of Chemistry and Biochemistry, University of California, Santa Cruz, Santa Cruz, CA.*
[7]*Department of Materials Science and Engineering, University of California at Berkeley, Berkeley, CA*
[8]*Department of Material Science and Engineering, Stanford University, Stanford, CA.*

Direct measurement of atomic coordinates in three dimensions is restricted to small specimens because the convergence angles required for atomic resolution in electron microscopy produce a shallow depth of focus [1]. Here we overcome this constraint using through-focal electron tomography, which combines focal and angular sampling to recover three-dimensional information throughout extended specimens. We used multislice simulations to establish reliable recovery beyond conventional depth-of-focus limits [2] [3]. Through-focal tomography therefore can extend atomic-coordinate measurements from isolated nanoscale objects to population-level analysis of large heterogeneous materials.

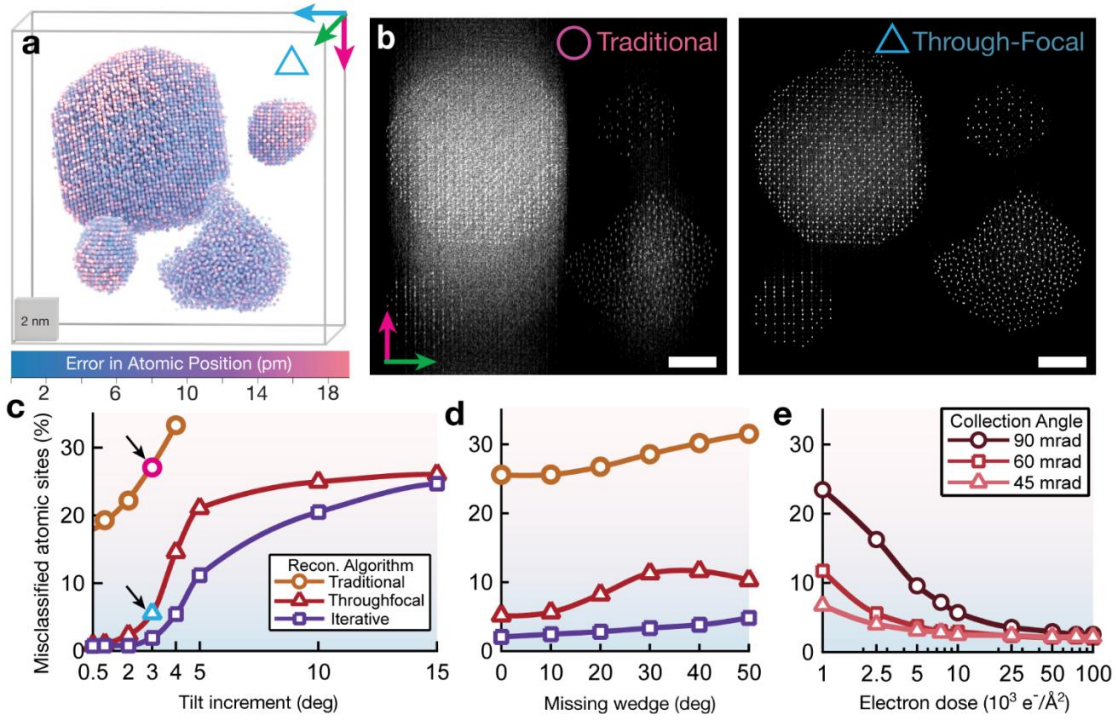


Fig. 1. Simulated Through-Focal Tomographic Reconstructions. a. Reconstructed coordinates colored by deviation from the ground-truth position (30° missing wedge, Δθ = 3°), scale cube 2 nm. **b.** Single-focus

traditional (left) and through-focal (right) reconstructions for the same sampling. Scale bars, 2 nm. **c-e**. Percent of misclassified atomic sites versus tilt increment, missing wedge and electron dose with arrows on plot c marking the two examples in **b.**

References:

1. Yalisove, R., Sung, S. H., Ercius, P. & Hovden, R. Limits of Three-Dimensional Resolution and Dose for Aberration-Corrected Electron Tomography. **Phys. Rev. Appl. 15**, 014003.https://doi.org/10.1103/PhysRevApplied.15.014003 (2021).
2. Kirkland, E. J. Advanced Computing in Electron Microscopy 3rd. ISBN: 978-3-030-33259-4. https://doi.org/10.1007/978-3-030-33260-0 (Springer International Publishing, Cham, Switzerland, 2020).
3. Ophus, C. A fast image simulation algorithm for scanning transmission electron microscopy. **Advanced Structural and Chemical Imaging 3**, 13. https://doi.org/10.1186/s40679-017-0046-1 (2017).

Geometrically Necessary Dislocation Density In 316l Stainless Steel Fabricated Via Laser Powder Bed Fusion

Justin Warner[1], Emily Konopka[2], Sriram Vijayan[1].*

[1] Materials Science and Engineering, Michigan Technological University, Houghton, MI, USA-49931

[2] Physics, Michigan Technological University, Houghton, MI, USA-49931

Laser Powder Bed Fusion (LPBF) is an advanced metal processing technology that can form net-shape components with complex geometries. The LPBF process involves spreading fine metallic powder across a substrate then melting portions of the powder with a high-powered laser. The process is performed layer-by-layer, adding thin layers of solidified metal to each iteration until a final stratified component is formed. The local heating and thermal cycling (layer additions) during LPBF create non-equilibrium conditions which result in metastable microstructural features in the final component [1]. For 316L Stainless Steel (SS), the LPBF process results in features which are accommodated by large densities of Geometrically Necessary Dislocations (GNDs) [2**].** These GNDs are quantifiable via lattice curvature measurements which can be obtained through electron backscatter diffraction (EBSD) techniques.

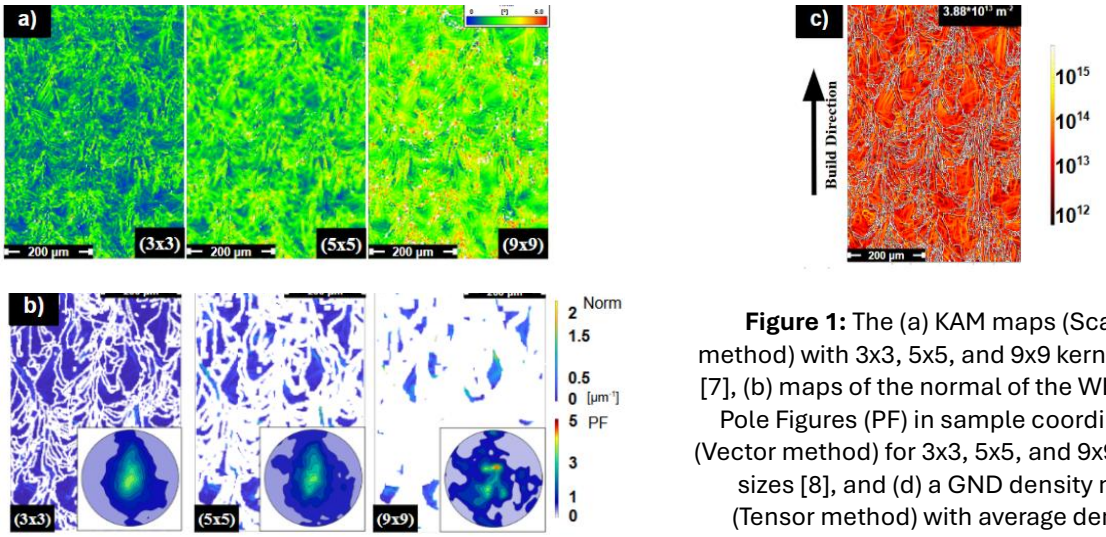


Figure 1: The (a) KAM maps (Scalar method) with 3x3, 5x5, and 9x9 kernel sizes [7], (b) maps of the normal of the WBV with Pole Figures (PF) in sample coordinates (Vector method) for 3x3, 5x5, and 9x9 kernel sizes [8], and (d) a GND density map (Tensor method) with average density indicated [8].

Three approaches to determining GND density from 2D EBSD data have been developed over the last two decades. Scalar value estimates of GND densities are obtained through Kernel Average Misorientation (KAM) data via energy conservation arguments [3,4]. Vectoral GND density estimates are obtained through the Weighted Burger's Vector (WBV) by taking the 2D data as a vector field and integrating over the surface to determine the weighted sum of the dislocations intersecting the area [5]. Tensorial methods to determine GND

density involve the point-based determination of lattice curvature which may be directly related to the GND density tensor [6]. Each methodology contains implicit assumptions which result in varied GND density values between the different data processing techniques. In this work, the KAM (Fig.1a), WBV (Fig.1b), and tensorial (Fig.1c) methods are used to determine GND densities in LPBF processed 316L SS. Nuances between methodologies are discussed and the resulting values and their variance are rationalized to understand the hetero-deformation arising from LPBF processing.

References

1. J. A. Warner and S. Vijayan. *Microscopy and Microanalysis* (2025) **volume 31** Supplement_1.https://doi.org/10.1093/mam/ozaf048.551

2. J. A. Warner, E. Konopka, V. Sriram. *Microscopy and Microanalysis* (2026) **volume32** Supplement_1.https://doi.org/10.1093/mam/ozag053.676

3. Q. Liu, D. Juul Jensen, N. Hansen. *Acta Materialia* (1998) **volume 46** 5819–5838. https://doi.org/10.1016/S1359-6454(98)00229-8

4. Y. Ateba Betanda, et al. *Materials Science and Engineering: A* (2014) **volume 614** 193–198. https://doi.org/10.1016/j.msea.2014.07.037

5. J. Wheeler, et al. *Journal of Microscopy* (2009) **volume 233** issue 3. https://doi.org/10.1111/j.1365-2818.2009.03136.x

6. W. Pantleon. *Scripta Materialia* (2008) **volume 58** 994–997. https://doi.org/10.1016/j.scriptamat.2008.01.050

Software:

7. Oxford Instruments. *AZtec Crystal*, version 4.0, [Software]. High Wycombe, UK: Oxford Instruments Nanoanalysis (2026).

8. F. Bachmann, R. Hielscher, H. Schaeben. *MTEX*, version 6.0.0, [Software] (2024). https://github.com/mtex-toolbox/mtex/releases/tag/mtex-6.0.0

Acknowledgements

Research performed at Michigan Technological University Materials Characterization and Fabrication Core Facility (RRID: SCR_027872) - Electron Microscopy core lab. The PI acknowledges the support from the Michigan Tech Start Up grant D97279

Hearing the Microscope: Experimental Characterization of Vibrations in High-Performance STEM

Kaia Thompson[1,], Suk Hyun Sung[1], Nishkarsh Agarwal[1], Eric Orson[2], and Robert Hovden[1,2]*

[1]Department of Materials Science and Engineering, University of Michigan, Ann Arbor, MI, USA

[2]Applied Physics Program, University of Michigan, Ann Arbor, MI, USA

In state-of-the-art STEM, achievable image quality is increasingly determined not by optical aberrations, but by environmental instabilities, including acoustic, mechanical, and electromagnetic disturbances[1,2,3]. These disturbances manifest as artifacts in STEM images, including periodic distortions of atomic features and satellite peaks and/or streaks in reciprocal space (Figure 1) [1,4]. Improving microscoperoom design to mitigate these disturbances requires understanding both the ambient environment and how vibrations couple to the microscope and degrade image quality.

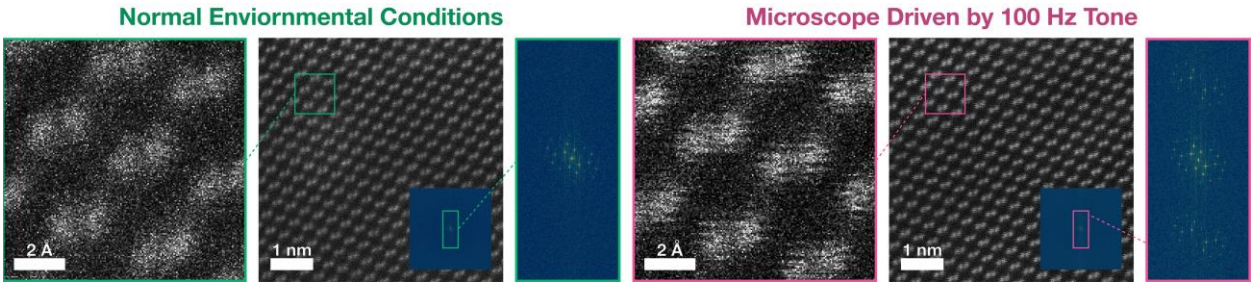


Fig. 1. STEM image and the amplitude of its Fourier transform under normal environmental conditions (left) and during acoustic excitation by a 100 Hz tone (right).

Here, we analytically describe how properties of environmental vibrations, including frequency and amplitude, determine the characteristics of the resulting STEM artifacts. We then develop a method for reconstructing these vibrations directly from STEM data. We compare these reconstructions with measurements from vibrometers mounted to various microscope components. While common features are observed across measurements, different components exhibit distinct responses to the same environmental disturbances. By measuring vibrations directly from STEM data, we can determine which vibrations couple strongly or weakly to image formation. This approach complements vibrometer measurements. Furthermore, we use a speaker to introduce controlled vibrations across a range of frequencies and examine their impacts on the microscope. Together, these measurements rigorously characterize imaging relevant instabilities and can guide targeted vibration mitigation.

References:

1. Jones L & Nellist PD. *Microscopy and Microanalysis* (2013) **19,** 1050–1060.

https://doi.org/10.1017/S1431927613001402

2. Muller DA et al. *Ultramicroscopy* (2006) **106**, 1033–1040.

https://doi.org/10.1016/j.ultramic.2006.04.017

3. Taurino A & Carlino E. *Materials* (2023) **16**, 1123. https://doi.org/10.3390/ma16031123

4. Li J et al. *Ultramicroscopy* (2018) 194, 167–174. https://doi.org/10.1016/j.ultramic.2018.07.011

Momentum-Resolved STEM Modalities for Polar Imaging of ScAlN Thin Films

Alex Stangel[1], Jeremy M. Shen[2], Danhao Wang[2], Zetian Mi[2], and Robert Hovden[1,3,]*
[1] Department of Materials Science and Engineering, University of Michigan, Ann Arbor, MI, United States
[2] Department of Electrical and Computer Engineering, University of Michigan, Ann Arbor, MI, United States
[3] Applied Physics Program, University of Michigan, Ann Arbor, MI, United States

Wurtzite ferroelectrics have garnered a large amount of attention recently due to their wide number of applications in areas such as electronics, piezoelectronics, and photonics [1-3]. Further, these materials exhibit a tunable coercive field and high remnant polarization, all while remaining seamlessly compatible with mainstream semiconductors [4-6]. These position wurtzite ferroelectrics as strong contenders for the next generation of electronics.

However, the underlying atomistic mechanisms at local length-scales behind the ferroelectric switching in wurtzites is poorly understood. To this end, scanning transmission electron microscopy (STEM) has proven to be an invaluable tool in analyzing the atomic structure of wurtzite ferroelectrics [7]. Further, recent advances in momentum-resolved imaging modalities such as integrated differential phase contrast (iDPC) and four-dimensional STEM (4D-STEM) have become routine and allow for mapping polarization in various material systems [8, 9].

Here, we utilize these momentum-resolved STEM imaging modalities to further explore and elucidate the latent polarization in ScAlN. Since iDPC imaging reveals information at the atomic scale (Fig. 1) and 4D-STEM at the nanoscale (Fig. 2), these two methods are complementary. We show that iDPC imaging and 4D-STEM can be utilized to provide information on the polarity of ScAlN thin films from the atomic scale up to the nanoscale.

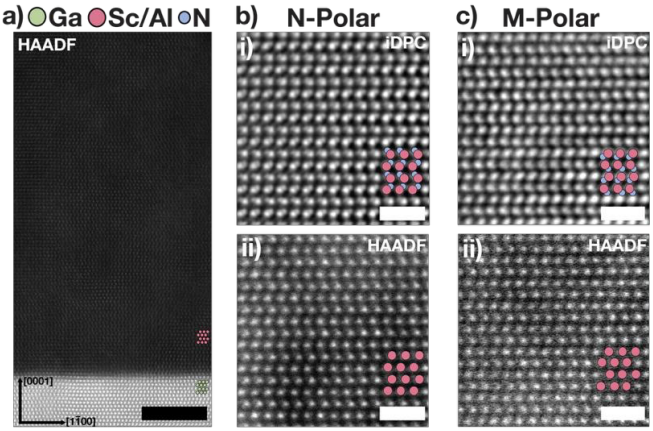


Fig. 1 (a) High-angle annular dark-field (HAADF) image of an MBE-grown ScAlN thin film grown on a GaN substrate (scale bar 5 nm). **b-c)** Zoomed-in iDPC **(i)** and HAADF **(ii)** images of N-polar and M-polar regions of the ScAlN film. Of note is HAADF cannot resolve the nitrogen atoms (and thus the polarity), whereas iDPC readily resolves the nitrogen (scale bars 1 nm).

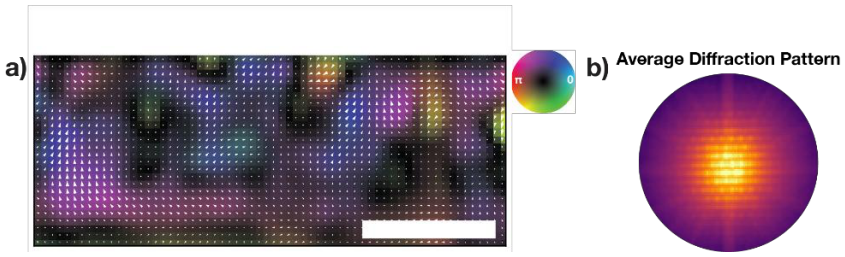


Fig. 2 (a) A 4D-STEM scan reveals the polarity of an M-polar ScAlN thin film. By scanning across the sample, the polarity direction and strength can be determined over hundreds of nanometer fields of view with nanoscale precision. Here, an M-polar film is expected to exhibit polarization primarily along the growth ([0001]) direction (scale bar 100 nm). The average diffraction pattern over the entire ScAlN film is shown in **(b)**.

References:

1. K. Kim *et al. Nat. Nanotechnol.* (2023) **18**, 422-441 https://doi.org/10.1038/s41565-023-01361-y
2. M. Akiyama *et al. Adv. Mater.* (2009) **21**, 593-596 https://doi.org/10.1002/adma.200802611
3. C. Xiong *et al. Nano Lett.* (2012) **12**, 3562-3568 https://doi.org/10.1021/nl3011885
4. S. Fichtner *et al. J. Appl. Phys.* (2019) **125**, 114103 https://doi.org/10.1063/1.5084945
5. J. Wang *et al. J. Microelectromech. Syst.* (2022) **31**, 234-240 https://doi.org/10.1109/JMEMS.2022.3147492
6. D. Wang *et al. Appl. Phys. Lett.* (2023) **122**, 052101 https://doi.org/10.1063/5.0136265
7. D. Wang, *et al. Nature* (2025) **641**, 76-82 https://doi.org/10.1038/s41586-025-08812-7
8. L. Caretta *et al. Nat. Mater.* (2023) **22**, 207-215 https://doi.org/10.1038/s41563-022-01412-0
9. A. Kumar *et al. Nat. Mater.* (2021) **20**, 62-67 https://doi.org/10.1038/s41563-020-0794-5

Cross-Platform Ultra-Cold Liquid Helium TEM Sample Holder with High Stability

Maya Gates[1,2], Nishkarsh Agarwal[3], Suk Hyun Sung[3,4], Emily Rennich[1,4], Benjamin H. Savitzky[2], Robert Hovden[2,3,5], and Ismail El Baggari[2,4]

[1.] *Department of Mechanical Engineering, University of Michigan, Ann Arbor, MI, USA*

[2.] *h-Bar Instruments, Ann Arbor, MI, USA*

[3.] *Department of Materials Science & Engineering, University of Michigan, Ann Arbor, MI, USA*

[4.] *Rowland Institute at Harvard University, Cambridge, MA, USA*

[5.] *Applied Physics Program, University of Michigan, Ann Arbor, MI, USA*

Here, we introduce a novel ultra-cold transmission electron microscope sample holder cooled with liquid helium capable of atomic resolution stability. This custom holder can reach any temperature between room and base cryogenic temperatures (≥23 K) in scanning transmission electron microscopes (S/TEM) with ±2 mK thermal stability over a period of 10+ hours [1].

Despite recent advancements in cryogenic TEM techniques and successes in atomic-resolution STEM studies at liquid nitrogen (LN_2) temperatures [2,3] and near liquid helium (LHe) temperatures [4,5], current tools are insufficient for materials characterization. Many radiation-sensitive materials and quantum phase transitions remain out of reach due to a lack of sufficiently stable ultra-cold capabilities. Additionally, severe thermal drift and mechanical vibrations caused by cryogen excitation yield low-quality images and short experimental windows for low-temperature side-entry sample holders [6]. Furthermore, LHe is orders of magnitude more volatile than LN_2, resulting in the exacerbation of current issues faced by side-entry holders at lower temperatures.

We have developed an ultra-cold specimen holder compatible with modern aberration-corrected TEMs to enable imaging of low-temperature phases of materials. This design incorporates vibration-damping equipment and a liquid-flow heat exchanger to reduce mechanical and thermal instability. These advancements enable atomic resolution imaging (≥0.8 Å) at ultra-cold temperatures (≥23 K). Precise temperature control is achievable with ±2 mK stability or better over long experiment windows (10+ hours), facilitating nanometer per minute (0.37 Å/s) sample drift. The holder design has been expanded to be compatible with JEOL, Thermo Fisher Scientific, and Bruker Nion microscopes.

In summary, our cryogenic TEM sample holder represents a significant advancement that addresses a longstanding desire to access ultra-cold temperatures within a modern aberration-corrected electron microscope, offering new opportunities for characterizing biological and quantum materials [7].

References

[1] E. Rennich et al., Proceedings of the National Academy of Sciences, **122**(36), e2509736122. doi: https://doi.org/10.1073/pnas.2509736122

[2] I. El Baggari et al., Proceedings of the National Academy of Sciences, **115**(7), p. 1445-1450. doi: 10.1073/pnas.1714901115

[3] B. H. Savitzky et al., Ultramicroscopy, **191**, p. 56–65. doi: 10.1016/j.ultramic.2018.04.008

[4] Y. Zhu, Accounts of Chemical Research, **54**(18), p. 3518-3528. doi: 10.1021/acs.accounts.1c00131
[5] J. Mun et al., Ultramicroscopy, **267**, p.114039. doi: 10.1016/j.ultramic.2024.114039
[6] B. H. Goodge et al., Microscopy and Microanalysis, **27**(1), p. 960-961. doi: 10.1017/S1431927621003652
[7] This work was supported by The Rowland Institute at Harvard and the University of Michigan. The authors are grateful for technical support from the Michigan Center for Materials Characterization.

Advancements in Targeted Ultramicrotomy for Correlative and Volume Electron Microscopy Workflows

Mercedeh Yeganeh, Ph. D.

Advanced Workflow Specialist – Sample Preparation, Leica Microsystems

Ultramicrotomy remains a critical yet challenging step in the preparation of biological and polymeric specimens for transmission electron microscopy (TEM) and volume electron microscopy (volume EM). Imprecise localization of subsurface regions of interest constrains data quality and reproducibility. This review examines emerging approaches in targeted ultramicrotomy that integrate multimodal imaging and coordinate mapping to enhance sectioning precision and workflow consistency.

Micro-computed tomography (micro-CT) guided trimming uses non-destructive volumetric X-ray imaging to localize embedded structures prior to sectioning. Spatial information derived from micro-CT datasets enables mapping between voxel coordinates and trimming trajectories, supporting selective material removal with improved accuracy. This approach reduces excess trimming and produces block faces aligned with the intended cutting plane.

Fluorescence-guided sectioning incorporates real-time optical imaging into the trimming and ultrathin sectioning process, enabling direct visualization of labeled structures within vitrified or resin-embedded samples. Continuous feedback during material removal allows for dynamic adjustment of block orientation and cutting depth and increases the likelihood of intersecting target structures at defined spatial coordinates. This method reduces operator-dependent variability and enhances early-section targeting efficiency in correlative light and electron microscopy (CLEM) workflows.

Together, these developments reflect a shift toward data-informed and feedback-enabled ultramicrotomy, where multimodal imaging improves targeting precision and overall workflow robustness in volume EM and CLEM applications.

Microstructural Characterization of 3D-Printed Silicon Anode Architectures for Advanced Batteries

Razia Sultana[1], Clare Simon[2], Jesse Stebbing[3] Paul L. Bergstrom[1]

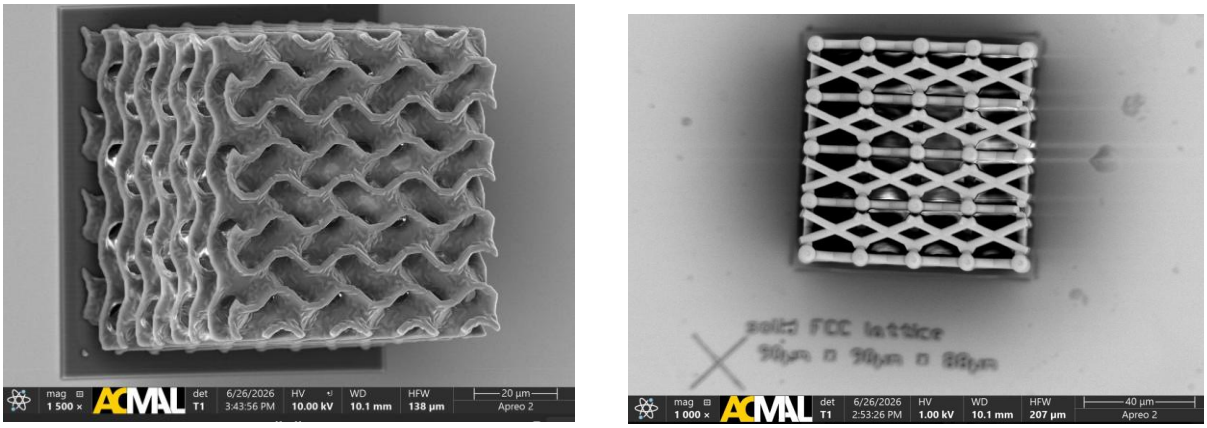
[1]Department of Electrical and Computer Engineering, Michigan Technological University, Houghton, MI, USA

[2]Department of Physics, Cornell University, Ithaca, NY, USA [3]Department of Physics and Astronomy, University of Nebraska-Lincoln, Lincoln, NE, USA

Silicon is a promising anode material for lithium- and sodium-ion batteries, offering a theoretical capacity approximately ten times greater than conventional graphite anodes. Its adoption is limited by a resulting volume expansion approaching ~300 % upon (de)lithiation, which drives particle fracture, loss of electrical contact, and unstable solid–electrolyte interphase growth. Porous silicon anode structures enable a reduction in the overall expansion volume to a great extent. Here we explore a deterministic approach to design the volumetric strain accommodation into the electrode architecture itself, using optimized morphology of different three-dimensional [1] scaffolds in which porosity, tortuosity, and ion transport path length are set by design rather than by powder packing.

Porous template scaffolds were fabricated by two-photon polymerization (2PP) on a Nano-scribe Photonic Professional GT2 in dip-in configuration, using a 63× objective and IP-Dip 2 photosensitive resin on p^{++} silicon substrates, followed by standard solvent development. Several design candidates, including gyroid, FCC, and BCC, are selected as primary design candidates for this work, as shown in Figure 1. Printed scaffolds are infiltrated with nanoparticles from a SiO_2/ethanol dispersion and pyrolyzed [2] in an inert atmosphere, converting the polymer template to glassy carbon while retaining the silica phase; a subsequent chemical vapor deposition step applies a carbon coating to render the filler electrochemically accessible. Print fidelity, shrinkage, and carbon quality are assessed by SEM imaging; ion transport and interfacial behavior are evaluated by electrochemical impedance spectroscopy and cyclic voltammetry in a three-electrode aqueous cell.

As Nanoscribe-based 3D printing enables the fabrication of complex microarchitectures with precise control over critical design parameters, it provides a promising pathway toward microanodes for on-chip batteries with rapid-charging capability. By treating electrode architecture as a controllable design variable rather than a consequence of conventional processing, this work establishes a route toward predictable and tunable ion transport, improved electrochemical performance, and high-capacity silicon anodes for next-generation microscale energy-storage systems.



(a) Gyroid **(b)** FCC

Figure 1: SEM imaging of three-dimensional microarchitectured electrode structures: (a) Gyroid and (b) FCC geometries.

References

[1] Guanjia Zhu, Dandan Luo, Xiaoyi Chen, Jianping Yang, and Haijiao Zhang. Emerging multiscale porous anodes toward fast charging lithium-ion batteries. *ACS nano*, 17(21):20850–20874, 2023.

[2] Aofei Mao, Hibiki Mitsuboshi, Maxime Trochon, Xiang Zhang, Lanh Trinh, Sedighe Keynia, Peixun Fan, Nada Kraiem, Xi Huang, Nan Li, et al. Evolution of chemical and mechanical properties in two-photon polymerized materials during pyrolysis. *Carbon*, 208:384–389, 2023.

Reaction-Time-Dependent Morphology of Solution-Grown 2D Lead Halide Perovskite Microplates

Jisna Abdul Razak[1], David Gordon[2], Jae Yong Suh[3]*

[1] Graduate Student, Michigan Technological University, Houghton, Michigan, United States

[2] Graduate Student, Michigan Technological University, Houghton, Michigan, United States

[3] Associate Professor, Michigan Technological University, Houghton, Michigan, United States

Layered organic-inorganic lead halide perovskite microplates are promising for optoelectronic applications because of their tunable electronic and optical properties. Such structures provide a platform for studying collective optical phenomena such as superfluorescence. The aim of this study is to obtain a thin film of 2D layered perovskite with well-defined microplate-like structures. This work investigates the solution-mediated formation of microplates from precursor films deposited on silicon substrates and subsequently immersed in a PEAI/isopropanol solution. The approach is inspired by reported dissolution-recrystallization procedures for producing 2D phenethylammonium lead-halide perovskite microplates[1]. Atomic force microscopy (AFM) was used to analyze microplate coverage, lateral size, overall height, and nanoscale surface morphology. Preliminary AFM studies showed that, after a 1 h reaction, isolated irregular crystallites with overall heights of approximately 100-120 nm were formed. Several crystallites exhibited secondary elevated areas with height differences of approximately 30-45 nm relative to surrounding regions. After 1.5 hours, more plate-like crystallites with concentric rings or terraces on their surfaces were observed. Although these structures show microplate-like morphology, their measured terrace heights are substantially larger than the approximately 1.7-3 nm thickness of an n=1 layered-perovskite repeat unit. Therefore, multilayered, stacked, or bulk-like structures may form rather than the intended 2D material. Further work aims to identify conditions for forming thinner structures with reduced step heights and controlled layer-by-layer microplate growth. Statistical AFM analysis will be performed at multiple substrate positions and across independently prepared samples. X-ray diffraction will be used to identify crystalline phases and orientation. Optical properties will be studied using steady-state photoluminescence, time-correlated single-photon counting, and femtosecond pump–probe spectroscopy to assess the potential for superfluorescence.

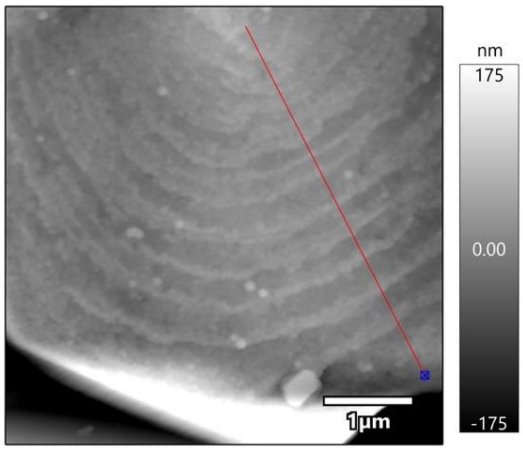


Fig.1. AFM height image of a plate-like crystallite after 1.5 h in PEAI/isopropanol. (The red line marks the height-profile location)

Reference:

1. Ma D, Fu Y, Dang L, Zhai J, Guzei IA, Jin S. Single-crystal microplates of two-dimensional organic–inorganic lead halide layered perovskites for optoelectronics. Nano Research (2017) 10(6): 2117–2129. https://doi.org/10.1007/s12274-016-1401-6

Multiscale Characterization of Lithium Depletion and Its Mitigation in High-Nickel Cathodes During Direct Recycling

Blessing Ozah[1] *and Lei Pan*[1,*]

[1]*Department of Chemical Engineering, Michigan Technological University, Houghton, Michigan, USA*

Direct recycling offers a promising route for recovering cathode active materials from end-of-life lithium-ion batteries while preserving their structure for reuse [1]. However, aqueous processing can induce lithium depletion and surface degradation that may remain undetected by conventional recovery metrics [2]. This study uses multiscale characterization to examine aqueous-induced changes in high-nickel cathodes and evaluate a lithium-rich strategy for mitigating lithium loss.

High-nickel cathode material was recovered by aqueous delamination and gravity separation. ICP-OES quantified lithium content; SEM-EDS and particle-size analysis evaluated morphology, elemental distribution, and particle size; XPS assessed surface composition and binder removal; XRD with Rietveld refinement evaluated crystal structure; and STEM-EELS probed surface and bulk chemical changes. Lithium-rich processing was subsequently applied to mitigate aqueous-induced degradation.

Gravity separation yielded a high-purity cathode concentrate (≈99%) while preserving spherical morphology, particle size (D50 ≈ 10 μm), and uniform Ni–Co–Mn distribution. XPS confirmed PVDF removal through disappearance of the CF_2 contribution in the C 1s spectrum. Despite successful recovery, ICP-OES revealed ≈15% lithium depletion. XRD showed *c*-axis contraction from 14.227 to 14.187 Å and increased Li–Ni cation mixing, consistent with delithiation (Fig. 1). STEM-EELS showed distinct surface–bulk differences after aqueous processing: surface nickel was reduced and the oxygen K-edge pre-peak was suppressed, while the bulk remained comparatively preserved (Fig. 2).

Lithium-rich processing mitigated these changes, restoring the *c*-axis toward the pristine value and minimizing surface–bulk differences in STEM-EELS spectra. These findings demonstrate its effectiveness in preserving the structural and chemical integrity of high-nickel cathodes during aqueous direct recycling.

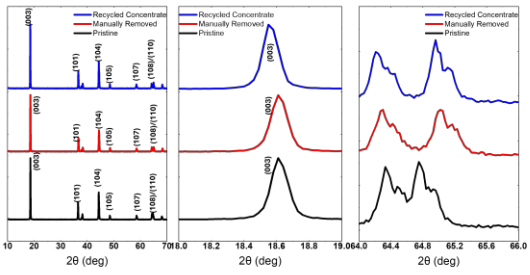


Fig. 1. XRD of pristine and recycled NMC811 showing (003) peak shift and c-axis contraction (14.227 to 14.187 Å), indicating lithium depletion after aqueous processing.

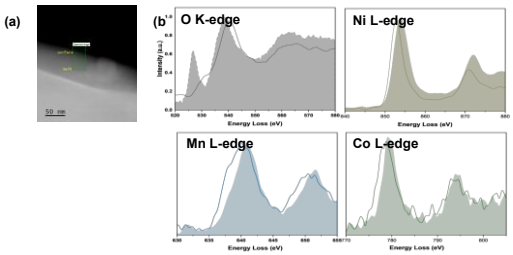


Fig. 2. STEM-EELS of processed NMC811. (a) HAADF-STEM image, surface and bulk regions marked (scale bar 50 nm). (b) O K, Ni L, Mn L, Co L edge spectra (surface solid, bulk shaded) showing surface Ni reduction and suppressed O K-edge pre-peak.

References

[1] Fan J, Luo H, Wang T, Dai S. Progress in direct recycling of spent lithium nickel manganese cobalt oxide (NMC) cathodes. *Energy Storage Materials* (2024) 73, 103813. DOI: 10.1016/j.ensm.2024.103813.
[2] Chen H, Mattsson A-M, King L, Liu H, Nielsen I, Ericson T, Preobrajenski A, Brant WR, Hahlin M. Study of degradation mechanisms in aqueous-processed Ni-rich cathodes for enhanced sustainability of batteries. *Journal of Materials Chemistry A* (2024) 12(37), 25393–25406. DOI: 10.1039/D4TA03592E.

Machine-Learning-Assisted Surface Plasmon Resonance Imaging for Quantitative Analysis of Droplet Evaporation

Andy Priskorn[1], Vaibhav Suryawanshi[1], and Chang Kyoung Choi[1,]*
[1]Department of Mechanical and Aerospace Engineering, Michigan Technological University, Houghton, Michigan, USA

Surface plasmon resonance (SPR) imaging uses light to examine changes at the interface between a metal surface and a sample. It is a label-free, noninvasive, and interface-sensitive optical imaging technique that detects local refractive-index changes near a thin metal film. By monitoring spatial variations in reflected light intensity with a camera, SPR imaging can visualize dynamic changes occurring at the liquid-solid interface. This capability makes SPR particularly useful for studying multicomponent droplet evaporation, where composition and interfacial conditions evolve over time.

For multicomponent droplets, differences in component volatility lead to selective evaporation and composition-dependent behavior. In ethanol-water mixtures, the more volatile ethanol evaporates preferentially, causing time-dependent changes in concentration, evaporation dynamics, and contact-line behavior [1,2]. Interactions between neighboring droplets and their spacing also affect evaporation [3]. To investigate these effects, droplet evaporation is visualized using bottom-view SPR imaging together with conventional side-view optical imaging. OpenCV automatically extracts geometric features, including projected area, diameter, centroid location, droplet height, baseline position, and contact angles. The analysis covers E10, E20, and E30 ethanol concentrations, single- and multiple-droplet configurations, and inter-droplet spacings of 1.1, 1.5, 1.8, and 2.0 mm.

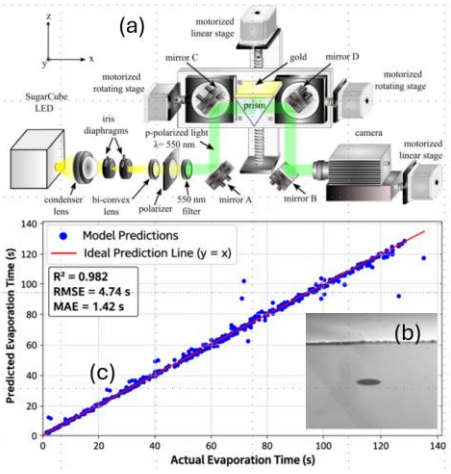


Fig. 1. (a) Schematic of the automated SPR imaging system, (b) representative SPR bottom-view image of an evaporating droplet, and (c) comparison of experimental and ML-predicted total evaporation time.

The extracted features are used with Linear Regression, Support Vector Regression (SVR), Random Forest, and XGBoost to predict evaporation progression and total evaporation time. Performance is evaluated using grouped cross-validation with R^2, RMSE, and MAE. XGBoost showed the strongest overall performance, achieving R^2 = 0.982, RMSE = 4.74 s, and MAE = 1.42 s for total evaporation-time prediction. Bottom-view SPR-derived features achieved prediction accuracy comparable to side-view optical imaging, demonstrating that the potential of SPR imaging combined with automated feature extraction and machine learning for quantitative predictions of droplet evaporation.

References:

1. Jeong CH, Lee HJ, Choi CK and Lee SH. *International Journal of Heat and Mass Transfer* (2021) 178 121584. https://doi.org/10.1016/j.ijheatmasstransfer.2021.121584
2. Jang KH, Yeom SH, Lee HJ, Choi CK and Lee SH. *International Journal of Heat and Mass Transfer* (2023) 207 124009. https://doi.org/10.1016/j.ijheatmasstransfer.2023.124009
3. Lee HJ, Choi CK and Lee SH. *International Communications in Heat and Mass Transfer* (2023) 146 106906. https://doi.org/10.1016/j.icheatmasstransfer.2023.106906

Microstructural and Mechanical Characterization of Combinatorial Tungsten-Copper Alloys Fabricated with Magnetron Sputtering

Aidan Earll[1], Sahil Pradhan[2], Sudarsanam Suresh Babu[2], Sriram Vijayan[1]*

[1]Michigan Technological University, Materials Science and Engineering, Houghton, MI, USA

[2]University of Maryland, Materials Science and Engineering, College Park, MD, USA

Tungsten-copper (WCu) alloys are of particular interest for fusion-relevant divertor applications due to their complementary high-temperature stability of tungsten and high thermal conductivity of copper [1,2]. The WCu system is immiscible under equilibrium conditions, making conventional bulk alloy processing particularly challenging. However, thin-film deposition methods such as magnetron sputtering provide access to metastable microstructures and compositional gradients unachievable with traditional processing routes [3]. These characteristics make WCu systems particularly relevant for combinatorial high-throughput screening approaches [4].

In this study, a combinatorial high-throughput synthesis approach was adopted to synthesize a binary WCu alloy thin film library spanning compositions of ~1-50 wt% copper. The fabricated alloys were characterized using scanning electron microscopy (SEM), energy dispersive spectroscopy (EDS), X-ray diffraction (XRD), and transmission electron microscopy (TEM) to investigate evolutions in film morphology with variations in composition. Mechanical and thermal properties were investigated with nanoindentation and four-point probe methods for assessment in extreme environments, relevant to fusion divertors. This work demonstrates the applicability of CHT synthesis for rapidly screening alloys and determining promising compositions for further development.

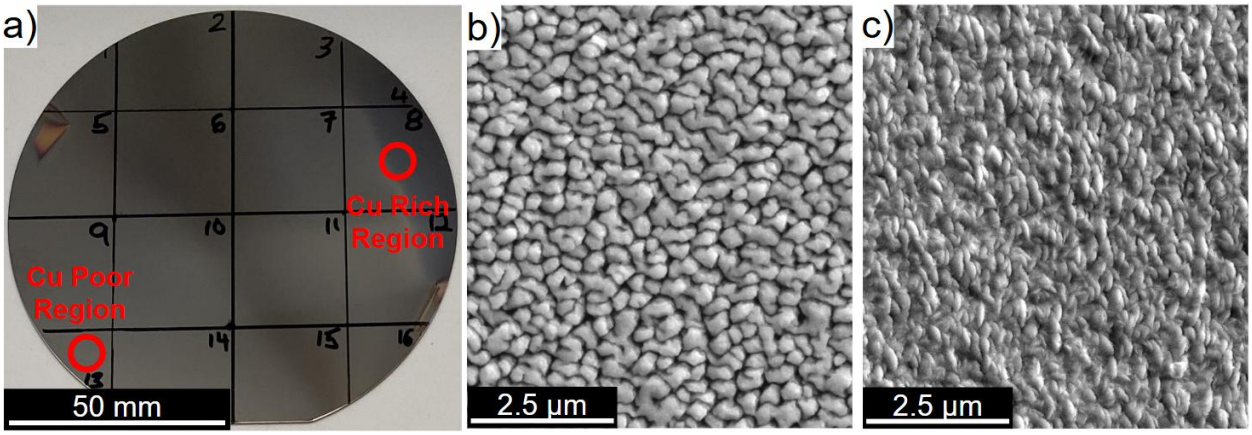


Fig. 1. The WCu a) fabricated combinatorial thin film and indicated (red circles) Cu rich and Cu poor regions and SEM micrographs from a b) copper rich region (~50wt% Cu) and c) copper poor region (~2 wt% Cu).

References:

1. Zinkle SJ and Was GS. *Acta Materialia* (2013) **61** 735–758. https://doi.org/10.1016/j.actamat.2012.11.004

2. Itoh Y, Takahashi M, and Takano H. *Fusion Engineering and Design* (1996) **31** 279–289. https://doi.org/10.1016/0920-3796(95)00432-7

3. Knotek O, Barimani A, and Löffler F. *MRS Online Proceedings Library* (1990) **187** 199–202. https://doi.org/10.1557/PROC-187-199

4. Hanak JJ. *Journal of Materials Science* (1970) **5** 964–971. https://doi.org/10.1007/BF00558177

Examination and Characterization of Cadmium Pigments and Paints

Eric Mattson, Hannah Campbell, and Lynn Mazzoleni

Michigan Technological University, Department of Chemistry, Houghton, MI, United States of America

Exploratory research was done on dry cadmium pigments and cadmium paint samples using a Hitachi TM4000 II Plus tabletop SEM. Cadmium pigments (e.g., CdS) are known semiconductor materials with sharply defined wavelength ranges and high total reflectance. These are desirable traits among pigments. We examined samples using SE and BSE detectors and characterized them with EDS mapping and point scans. We prepared samples as a suspension in alcohol and placed them on conductive carbon tape with an aluminum backing. The goal of this work was to examine pigment particle size and morphology to see whether they affected color. The cadmium pigments showed variable degrees of clustering, which appeared to relate to the approximate pigment concentration in suspension. We also examined the semiconductor chemistry using EDS mapping. The chemistry appears to play the primary role in causing color, with band gaps blue-shifted when Cd is substituted with Zn and red-shifted when S is substituted with Se. However, particle size and morphology may still play an important role when comparing cadmium pigments with other pigment classes.

Microstructural analysis of bronze coinage from the Seleucid Empire

Daniel H. Branagan[1], Joshua Mueller[1], Caleb Stetson[1]

[1]Michigan Technological University, Materials Science and Engineering, Houghton, Mi, USA

Bronze coinage from the Seleucid Empire is well documented in numismatic literature, yet little archaeometallurgical work has been conducted on these artifacts. Certain Seleucid bronze coins exhibit distinctive serrated or "bottle-cap" edges whose manufacturing method remains uncertain. This study examines fourteen Seleucid bronze coins from a legally exported private collection, five of which were selected for destructive analysis. Alloy composition, microstructure, and thermal behavior were characterized using ICP-OES, optical and scanning electron microscopy, EDS, and DSC/TGA. The analyzed coins contained 77.62-89.12 wt.% Cu, 6.06-17.12 wt.% Pb, and 2.69-4.82 wt.% Sn. Their predominantly dendritic microstructures indicate that the flans remained largely as cast, while the Pb-rich regions were consistent with monotectic liquid-phase separation and late-stage lead solidification. In the serrated coin, the columnar solidification region along the edge did not follow the serration contours, indicating that the serrations were produced by mechanical deformation after casting rather than formed in the flan mold. These results provide insight into alloy solidification, flan production, and serrated-edge formation in Seleucid bronze coinage.

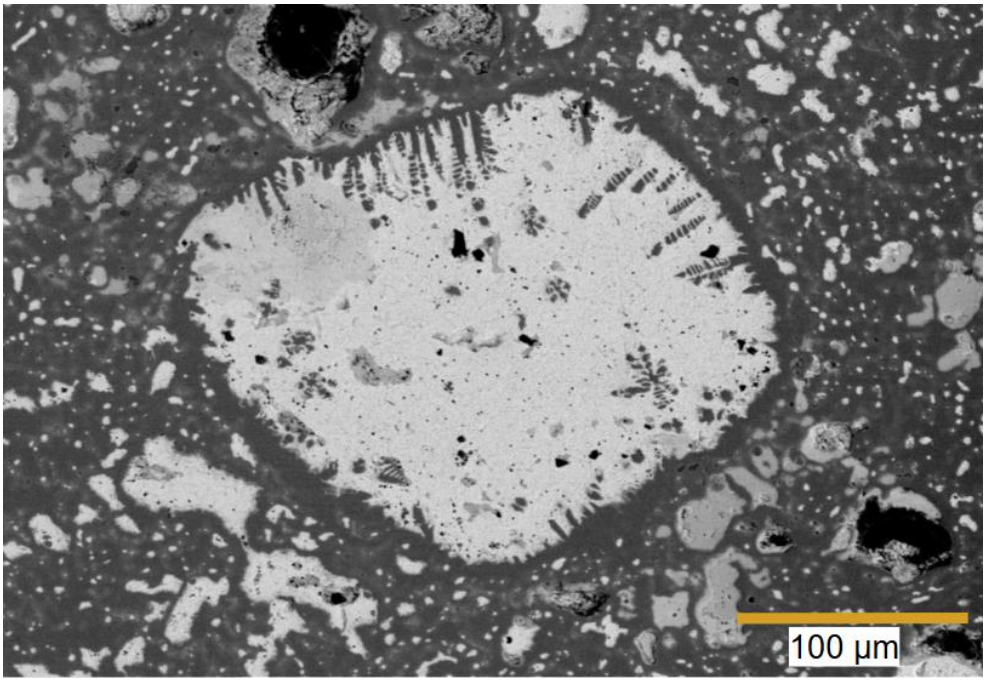


Fig 1. Backscatter electron image of the microstructure of a Seleucid Empire Cu-Sn-Pb bronze coin (approx 2300 years old).

Contrast-Enhanced Ultrasound Localization Microscopy for Evaluating and Characterizing Surface-Connected Defects in Steel

Raliba Hinga Roseline[1], Quang Tran[1], and Moira Brandstetter [2**]*
[1]Michigan Technological University, Civil, Environmental, and Geospatial Engineering, Houghton, MI, USA
[2]Michigan Technological University, Biological Sciences, Houghton, MI, USA

Single-molecule localization microscopy techniques (e.g., PALM/ STORM) achieve super-resolution by localizing the centers of many individual, spatially isolated emitters over time. This work explores the same principle to evaluate surface-connected defect geometries that conventional ultrasound cannot fully resolve using ultrasound localization microscopy (ULM) combined with contrast-enhanced ultrafast ultrasound imaging as a nondestructive evaluation technique in steel.

Microbubble contrast agents (CA) smaller than the ultrasonic resolution limit were introduced into the defect channels and imaged as they flowed through the flaws. Individual CA exhibited spatially extended, system-dependent point-spread responses in the ultrasound images rather than appearing at their true physical size. By localizing the centers of the CA responses across successive frames, accumulating their positions, and tracking the flow path, we reconstructed the defect geometry.

Steel specimens with artificially created EDM (Electrical Discharge Machining) vertical and inclined cracks with depths of 1, 3.5, and 5 mm and a width of 0.4 mm were used to test the technique. The known specimen geometries were compared with the reconstructed crack width, depths, and inclinations. The inclination-angle errors were less than 1%, while the reconstructed depths had relative errors below 10%.

These results show that quantitative, sub-resolution geometric information of the defects, normally obtainable only by sectioning or otherwise damaging a sample, can be obtained nondestructively by localizing, tracking, and accumulating individual particle responses. This method offers a foundation to evaluate irregularities and defects in steels and expands localization microscopy to the nondestructive assessment of engineering materials.

Correlating Nanoscale Structure and Magnetic Behavior in Artificial Spin Ice Using Integrated AFM and SEM

S. Ladva[1]

[1] *Quantum Design Inc., San Diego, CA, USA, satyam@qdusa.com*

Artificial spin ice consists of lithographically patterned arrays of interacting nanoscale magnetic elements exhibiting geometrical frustration and collective magnetic behavior. Their magnetic response is strongly influenced by nanomagnet geometry, dimensions, surface morphology, and fabrication-induced defects. Correlating structural and magnetic properties is therefore important for understanding their behavior.

Here, we demonstrate a correlative microscopy approach combining scanning electron microscopy (SEM), atomic force microscopy (AFM), and magnetic force microscopy (MFM) to characterize artificial spin ice nanostructures. SEM provides lateral geometry and pattern fidelity, while AFM provides complementary topographical information including height, morphology, and roughness. Integrating AFM within the SEM enables measurements at the same region of interest without sample transfer.

SEM imaging also enables identification of individual nanostructures and guides AFM probe placement. MFM subsequently provides nanoscale magnetic contrast from individual nanoislands, allowing structural features to be correlated with local magnetic configurations. Measurements demonstrate dipolar magnetic contrast predominantly consistent with single-domain states, together with more complex local features.

This correlative approach connects nanoscale geometry, topography, defects, and magnetic behavior within the same structures, providing a pathway for linking nanofabrication with the characterization and optimization of magnetic and quantum-material systems.

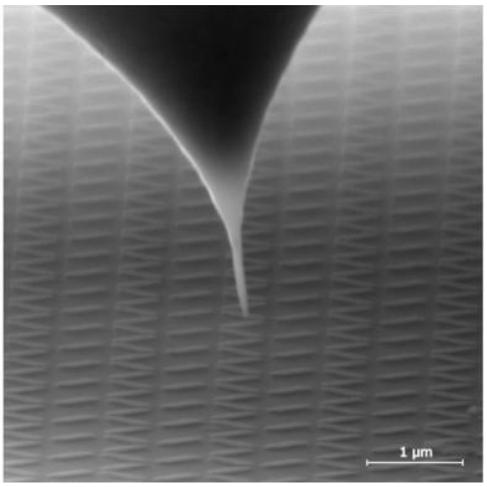


Figure 1. SEM-guided positioning of the AFM probe over an artificial spin ice array, enabling site-specific correlative nanoscale characterization.

References

[1] R. F. Wang *et al.*, Nature **439**, 303–306 (2006).

[2] S. H. Skjærvø *et al.*, Nat. Rev. Phys. **2**, 13–28 (2020).

[3] Quantum Design, *Artificial Spin Ice: A Cross-Platform Analysis*, Application Note.

AUTHOR/TITLE INDEX

Physicochemical Properties of Biomacromolecules Measured by Atomic Force Microscopy 5

Caryn L. Heldt **5**

Computational Imaging of the Tumor Microenvironment 7

Characterization of materials and biological samples by transmission electron microscopy 9

Unlocking the Mechanisms of Phase Transformations in Complex Metallic Alloys via In Situ TEM Heating – From Sample Preparation to Temperature Calibration and Data Interpretation 11

Sriram Vijayan **11**

Gas Cell TEM and Its Applications in Materials Science 13

Xiaobing Hu **13**

Advancing Electron Ptychography: From High-Performance Reconstruction to AI-Enhanced 3D Imaging 14

Chia-Hao Lee[1] **14**

Quantitative Imaging of Structure and Viability in *Staphylococcus epidermidis*-Infected Fibrin Clots Under Heated Perfusate 15

Linqi Huang **15**

Scanning Electron Microscopy Characterization of Surface Coverage and Thrombus Infiltration in Novel Coated ePTFE Vascular Grafts 17

Oscar Moreno **17**

Spatiotemporal Analysis of FAK Phosphorylation and Vinculin Dynamics Reveals Two Distinct Stiffness-Dependent Mechanotransduction Pathways in Cancer Cells 19

Majid Rostami **19**

Graph Theoretical Relationships for Chiroptical Activity for Gold Nanorods with Complex Corrugated Geometry 21

Jessica Ma **21**

Damage of Beam-Sensitive Organics from Room Temperature to Liquid Helium 23

Jason Manassa **23**

Tailoring the plasmonic properties of InGa alloy nanoparticle arrays 25

Hailey McKenna **25**

Advances in Detector Technologies for Materials Science: From Low-Dose Imaging to 4D STEM 27

Anahita Pakzad **27**

Super-X G3: Higher Light-Element Sensitivity and Faster Compositional Mapping at Analytical Beam Currents 28

Austin Wade **28**

Evaluating the Brittle-to-Ductile Transition of Silicon by *in situ* Nanomechanics 29

Eric D. Hintsala **29**

Cy5-PEG4 Enables Blood–Brain Barrier-Penetrant Imaging of Mitochondrial Dynamics in Neuronal Systems 35

Muhammad Bilal Umar **35**

Real-Time Visualization of Mitophagy Flux by Reversible Mitochondrial Redox Fluorescence Imaging 37

Brayden Storey **37**

Multiscale Correlative Microscopy of Surface-Engineered Silver Nanoparticles: From Nanoscale Architecture to In Vitro and In Vivo Label-Free Bio-Tracking 38

Jije Geyesa **38**

Specific Protein Nanoparticle Crosslinking for Protein Delivery 40

Kate Kaplin **40**

Microscopic Characterization and In Vivo Vascular Response of Polydopamine-Cu(II)-Coated Biodegradable Zinc 42

Md Tanvir Hossain **42**

A Novel Method to Vascularize Organoids Using Microfluidic Devices 45

Viviana Secci **45**

MitoGlow-ROS Enables High-Dynamic-Range, Multi-Scale Fluorescence Imaging of Mitochondrial Oxidative Stress from Cells to Brain Tissue 47

Jake Williams **47**

Anion-Directed Self-Assembly of Copper Iodide-Penicillamine Frameworks: Tuning Morphology and Chiroptical Properties 49

Riva Akter **49**

Integrative Microscopy Delineates Biogenesis and Self-Assembly of Extracellular Matrix Polymers in Diatoms 50

Michael R. Gretz **50**

Single-particle characterization of mechanical and surface properties of empty and full AAV9 Capsids using atomic force microscopy 51

Vaishali Sharma **51**

Measuring the Three-dimensional Coordinates of Atoms with Through 52

Focal Electron Tomography 52

Eric M. Orson **52**

Geometrically Necessary Dislocation Density In 316l Stainless Steel Fabricated Via Laser Powder Bed Fusion 54

Justin Warner **54**

Hearing the Microscope: Experimental Characterization of Vibrations in High-Performance STEM 56

Kaia Thompson **56**

Momentum-Resolved STEM Modalities for Polar Imaging of ScAlN Thin Films 58

Alex Stangel **58**

Cross-Platform Ultra-Cold Liquid Helium TEM Sample Holder with High Stability 60

Maya Gates **60**

Advancements in Targeted Ultramicrotomy for Correlative and Volume Electron Microscopy Workflows 62

Mercedeh Yeganeh **62**

Microstructural Characterization of 3D-Printed Silicon Anode Architectures for Advanced Batteries 63

Razia Sultana **63**

References **64**

Reaction-Time-Dependent Morphology of Solution-Grown 2D Lead Halide Perovskite Microplates 65

Jisna Abdul Razak **65**

Multiscale Characterization of Lithium Depletion and Its Mitigation in High-Nickel Cathodes During Direct Recycling 67
Blessing Ozah **67**
Machine-Learning-Assisted Surface Plasmon Resonance Imaging for Quantitative Analysis of Droplet Evaporation 69
Andy Priskorn **69**
Microstructural and Mechanical Characterization of Combinatorial Tungsten-Copper Alloys Fabricated with Magnetron Sputtering 71
Aidan Earll **71**
Examination and Characterization of Cadmium Pigments and Paints 73
Eric Mattson **73**
Microstructural analysis of bronze coinage from the Seleucid Empire 74
Daniel H. Branagan **74**
Contrast-Enhanced Ultrasound Localization Microscopy for Evaluating and Characterizing Surface-Connected Defects in Steel 75
Raliba Hinga Roseline **75**
Correlating Nanoscale Structure and Magnetic Behavior in Artificial Spin Ice Using Integrated AFM and SEM 76
S. Ladva **76**

MEETING COMMITTEE



Committee Chair
Ellen Keene
DuPont

Life Sciences Director
Jing Liang
University of Michigan





Physical Sciences Director
Zehao Li
University of Michigan

Vendor Liaison
Vickie Kimler
Wayne State University (retired)





Webmaster
Alyssa Fielitz
Dow Chemical Company

Local Arrangement Chair
Erico Freitas
Michigan Technological University





Current President
Tao Ma
University of Michigan

Great Lakes Microscopy Society thanks

ThermoFisher SCIENTIFIC

GATAN

BRUKER

1885

ħ-bar instruments

Michigan Tech

HITACHI
Inspire the Next

Thomas Scientific

Leica MICROSYSTEMS

CIQTEK

Tescan

for making our annual meeting possible